

UNIVERSITÉ DU QUÉBEC À MONTRÉAL

THE ROLE OF NITROGEN, OXYGEN, AND CARBON IN THE GROWTH
OF LARGE-AREA GRAPHENE MONOLAYER ON COPPER CATALYST

THESIS
PRESENTED
AS PARTIAL REQUIREMENT
FOR THE DEGREE MASTER OF CHEMISTRY

BY
FILIP BOGDAN POPESCU

DECEMBER 2015

UNIVERSITÉ DU QUÉBEC À MONTRÉAL
Service des bibliothèques

Avertissement

La diffusion de ce mémoire se fait dans le respect des droits de son auteur, qui a signé le formulaire *Autorisation de reproduire et de diffuser un travail de recherche de cycles supérieurs* (SDU-522 – Rév.07-2011). Cette autorisation stipule que «conformément à l'article 11 du Règlement no 8 des études de cycles supérieurs, [l'auteur] concède à l'Université du Québec à Montréal une licence non exclusive d'utilisation et de publication de la totalité ou d'une partie importante de [son] travail de recherche pour des fins pédagogiques et non commerciales. Plus précisément, [l'auteur] autorise l'Université du Québec à Montréal à reproduire, diffuser, prêter, distribuer ou vendre des copies de [son] travail de recherche à des fins non commerciales sur quelque support que ce soit, y compris l'Internet. Cette licence et cette autorisation n'entraînent pas une renonciation de [la] part [de l'auteur] à [ses] droits moraux ni à [ses] droits de propriété intellectuelle. Sauf entente contraire, [l'auteur] conserve la liberté de diffuser et de commercialiser ou non ce travail dont [il] possède un exemplaire.»

UNIVERSITÉ DU QUÉBEC À MONTRÉAL

THE ROLE OF NITROGEN, OXYGEN, AND CARBON IN THE GROWTH
OF LARGE-AREA GRAPHENE MONOLAYER ON COPPER CATALYST

MÉMOIRE
PRÉSENTÉ
COMME EXIGENCE PARTIELLE
DE LA MAÎTRISE EN CHIMIE

PAR
FILIP BOGDAN POPESCU

NOVEMBRE 2015

ACKNOWLEDGEMENTS

First, I would like to thank my supervisor, Professor Mohamed Siaj, and my co-supervisor, Professor Ricardo Izquierdo, who welcomed and supported me in their team. Moreover, my work could not have advanced without the aid of Doctor Abdeladim Guermoune whose expertise and insight inspired me from my time as an undergraduate up to the first year of my M.Sc.

I extend my gratitude to my jury, Pr. Jerome. Claverie from the University of Quebec in Montreal (UQAM), and Pr. Fiorenzo Vetrone from the National Institute of Scientific Research (INRS) who took their time to judge my work.

The list could not be complete without thanking my colleagues, especially Jeanne N'Diaye, Farzaneh Mahvash, Mansouria Zidi, and Gaston Contreras who supported me through the best of times and the worst of times. Among my non-academic friends I wish to thank Damien Dargent whose music taste, encouragements, and support brought me precious moments of solace and flow.

Most importantly, I thank my family for their support through what was the most enriching experience of my life so far.

CONTENTS

LIST OF TABLES	vi
LIST OF FIGURES	vii
ABSTRACT	xi
ABSTRACT	xii
INTRODUCTION	1
0.1 Carbon Allotropes and Nanocarbons	1
0.2 Applications and Perspectives	4
0.3 Conclusion	5
CHAPTER I .	
CHARACTERIZATION METHODS	6
1.1 Atomic Force Microscopy	6
1.1.1 Microscope	7
1.1.2 Operating modes	8
1.1.3 Other analysis	10
1.2 X-Ray Photoelectron Spectroscopy	10
1.2.1 Electronic Spectroscopy	11
1.2.2 Interpretation	11
1.2.3 Identifying the chemical state	12
1.3 Scanning Electron Microscopy and Transmission Electron Microscopy	14
1.3.1 Scanning Electron Microscopy	15
1.3.2 Secondary Electron Imaging	15
1.3.3 Backscattered Electron Imaging	16
1.4 Raman	16
1.4.1 Raman Fingerprint of some Carbon allotropes	17

1.5	Conclusion	20
CHAPTER II		
GRAPHENE GROWTH FROM METHANE AND ALIPHATIC ALCOHOLS		21
2.1	Graphene, introduction	21
2.2	Graphene synthesis methods	22
2.2.1	Exfoliation	22
2.2.2	SiC epitaxy	23
2.3	Chemical Vapour Deposition graphene growth	23
2.3.1	Chemical Vapour Deposition systems	24
2.3.2	CVD graphene growth process	24
2.4	Synthesis from alcohols	28
2.4.1	Experimental procedure	29
2.4.2	Characterization	30
2.5	Conclusion	36
CHAPTER III		
N-GRAPHENE GROWTH FROM NITROGEN CONTAINING PRECURSORS		37
3.1	Doped graphene	37
3.2	Characterization and discussion	39
3.2.1	XPS	39
3.2.2	Raman	43
3.3	Conclusion	44
CHAPTER IV		
EFFECT OF THE SIMULTANEOUS PRESENCE OF OXYGEN, CARBON, AND NITROGEN MOIETIES DURING CVD GRAPHENE GROWTH		46
4.1	Preliminary results	46
4.2	Results and discussion	47
4.2.1	XPS	48
4.2.2	SEM imagery	50

4.2.3 Raman	55
4.3 Conclusion	57
CONCLUSION	58
APPENDICE A XPS SPECTRA OF VARIOUS SAMPLES HAVING PASSED THROUGH A CVD REACTION	60
BIBLIOGRAPHY	67

LIST OF TABLES

Tableau	Page
4.1 Atomic ratios (C:N:O) for the different precursors used.	47

LIST OF FIGURES

Figure	Page
1.1 AFM cantilever and tip assembly schematic.(Frétigny, 2005) . . .	7
1.2 Surface-tip interaction curve.(Frétigny, 2005)	8
1.3 C1s high resolution XPS spectra of graphite, nanodiamond, and graphite with increasing laser power treatment. Adapted from Mérel et al. 1998.	14
1.4 Electron beam source. Illustrated, a field emission filament tip cathode and the anodes responsible for the electron extraction.(of Iowa,)	15
1.5 Comparison of Raman spectra at 514 nm for bulk graphite and graphene; scaled to illustrate a similar height of the 2D peak around 2700 cm ⁻¹ .(Ferrari <i>et al.</i> , 2006)	18
1.6 The crystal structure of graphite. Illustrated, its primitive unit cell, with dimensions $a = 2.46 \text{ \AA}$ and $c = 6.71 \text{ \AA}$, and an in-plane bond length of 1.42 Å. A , A' , B , and B' are the four atoms forming graphite's unit cell. Atoms A and A' (full circles) have neighbours directly above and below in adjacent layer planes; B and B' (open circles) have neighbours directly above and below in layer planes 6.71 Å away.(Chung, 2002)	19
2.1 Schematic representation of the used CVD system.(Guermoune <i>et al.</i> , 2011).	24
2.2 Micro-Raman characterization of the isotope-labeled graphene grown on Cu foil and transferred onto a SiO ₂ /Si wafer. Integrated intensity Raman maps of (d) G_{13+12} (1500 cm ⁻¹ to 1620 cm ⁻¹), (e) G_{13} (1500 cm ⁻¹ to 1560 cm ⁻¹), and (f) G_{12} (1560 cm ⁻¹ to 1620 cm ⁻¹). Scale bars are 5 μm.(Li <i>et al.</i> , 2009b)	26
2.3 Schematic representation of the transfer procedure of graphene grown on copper foils.(Lee, 2013)	27

2.4	C1s XPS data for alcohol and methane grown graphene. No oxygen-doped peak was observed for pristine graphene.	31
2.5	SEM images of graphene on 25 μm Cu foil substrates, compared for growth by (a) methanol (b) ethanol (c) 1-propanol and (d) gas source methane. The images show the presence of Cu surface steps, and graphene wrinkles which result from the difference between the thermal expansion coefficient of graphene and Cu, indicating that the graphene film is continuous and uniform.	32
2.6	A $3 \times 3 \text{ cm}^2$ CVD graphene film grown using methanol, transferred to a SiO_2/Si substrate.	33
2.7	Raman spectra of a transferred CVD graphene film on SiO_2/Si compared for growth by methanol, ethanol and 1-propanol. The small D peak (1350 cm^{-1}) and the intensity of the $2D$ peak (2700 cm^{-1}) found to be more than twice as high as the G peak (1580 cm^{-1}) indicate the presence of high quality monolayer graphene.	34
2.8	Raman spectra of transferred CVD graphene compared by precursor and growth temperature. A Renishaw inVia spectrometer, 514.5 nm laser wavelength, and 100x objective lens was used. (A) With a temperature increase from $650 \text{ }^\circ\text{C}$ to $850 \text{ }^\circ\text{C}$, the intensity of the D peak (1350 cm^{-1}) decreases and the $2D$ peak sharpens, indicating a reduction in defect density and improved graphene quality. (B) Evolution of the D band with temperature, noting the fit of two Lorentzians ($650 \text{ }^\circ\text{C}$) turning into one at $850 \text{ }^\circ\text{C}$, characteristic of monolayer graphene. (C) No significant difference is observed in D peak integrated intensity versus alcohol precursor.	35
3.1	XPS characterization of N-doped graphene grown up to 30 minutes. C1s and N1s core-level X-ray photoelectron spectra of grown graphene from : a) ethylenediamine b) N-methylimidazole. The C1s peak can be split to three Lorentzian peaks labeled by red, blue, and green lines corresponding to graphite-like $sp^2 \text{ C}$, $\text{N}_{sp^2} - \text{C}$ bond and CO (due to absorbed oxygen) respectively. The N1s peak can be split to Lorentzian corresponding to pyridinic, pyrrolic and graphitic forms labeled by red, blue and green lines respectively. .	40

3.2	XPS characterization of N-doped graphene grown up to 30 minutes from a) pyridine, and b) dimethyleformamide. The C1s peak can be split to three Lorentzian peaks labeled by red, blue, and green lines corresponding to graphite-like sp^2 C, $N_{sp^2} - C$ bond and CO (due to absorbed oxygen) respectively. The N1s peak can be split to Lorentzian corresponding to pyridinic, pyrrolic and graphitic forms labeled by red, blue and green lines respectively.	41
3.3	SEM image of a) the fast nucleation after 3 minutes of growth on copper, the second and third layers are seen clearly over the first layer. b) Transferred film grown from ethylenediamine after 30 min at 5 Torr of H_2 pressure, large domains of bilayer, trilayer and multilayer over monolayer within several microns cover silicon dioxide. c) At 8 Torr of H_2 a few domains of bilayer N-doped graphene are seen on transferred film on silicon dioxide. d) Monolayer of N-doped graphene transferred on silicon dioxide using 10 Torr of hydrogen in the growth.	42
3.4	Raman spectra of monolayer N-doped graphene using precursors: pyridine, dimethylformamide, N-methylimidazole and ethylenediamine. The measurements were performed on films transferred on silicon dioxide.	44
4.1	C1s and N1s XPS spectra of copper samples after CVD reaction with nitromethane.	49
4.2	SEM image of a copper sample after having been exposed to a 15 minute CVD reaction with nitromethane.	50
4.3	SEM image of a copper sample after having been exposed to a 30 minute CVD reaction with nitromethane.	51
4.4	SEM image of a copper sample after having been exposed to a 45 minute CVD reaction with nitromethane.	52
4.5	SEM image of a copper sample after having been exposed to a 60 minute CVD reaction with nitromethane.	53
4.6	SEM image of a copper sample after having been exposed to a 75 minute CVD reaction with nitromethane.	54
4.7	Average hole diameter versus CVD growth time on copper samples using nitromethane as a precursor. Sample sizes of 10 (for 15 minutes) and 63 holes (30, 45, 60, 75 minutes).	54

4.8	Mass loss statistics of 8 samples per reaction duration (15, 45, 60, 75 minutes), for nitromethane and methane sourced CVD reactions. For visualization convenience, mean error bars were multiplied by a factor of 1000 for CH ₄ , 100 for CH ₃ NO ₂ and the last data point at 75 °C by a factor of 10.	55
4.9	Two Raman spectra after a 15 minutes nitromethane-sourced CVD reaction on copper samples.	56
4.10	Raw Raman spectral data on copper samples having passed through a CVD growth using a) nitromethane and b) EDA/H ₂ O mixture for a duration of 2 hours. Only the copper's Raman background is visible.	56
4.11	Raman spectra on copper samples after standard CVD reactions with methane, benzene, phenol, aniline, and nitrobenzene; performed under similar conditions as the methane growth.	57
A.1	C1s XPS of benzene-sourced CVD sample.	60
A.2	N1s XPS of benzene-sourced CVD sample.	61
A.3	O1s XPS of benzene-sourced CVD sample.	61
A.4	C1s XPS of aniline-sourced CVD sample.	62
A.5	N1s XPS of aniline-sourced CVD sample.	62
A.6	O1s XPS of aniline-sourced CVD sample.	63
A.7	C1s XPS of nitrobenzene-sourced CVD sample.	63
A.8	N1s XPS of nitrobenzene-sourced CVD sample.	64
A.9	O1s XPS of nitrobenzene-sourced CVD sample.	64
A.10	C1s XPS of phenol-sourced CVD sample.	65
A.11	N1s XPS of phenol-sourced CVD sample.	65
A.12	O1s XPS of phenol-sourced CVD sample.	66

ABSTRACT

THE ROLE OF NITROGEN, OXYGEN, AND CARBON IN THE GROWTH OF LARGE-AREA GRAPHENE MONOLAYER ON COPPER CATALYST

Since its isolation in 2004 graphene persistently remains a synthesis challenge. In order to take advantage of its full potential, high quality samples are required, *i.e.* large surfaces of mono-crystalline graphene. The Chemical Vapour Deposition growth method is one of the synthesis methods capable of satisfying those needs. Moreover, graphene's chemical *n*-doping opens its application potential.

Using copper sheets as catalyst and several aliphatic precursors as carbon source, variable qualities of graphene can be produced. Methane and acetylene remain the most popular precursors. In this work it is shown that graphene synthesis from aliphatic alcohols (methanol, ethanol, 1-propanol) is possible, and that the presence of oxygen doesn't influence the quality of the final product. Moreover, doped graphene is achieved using precursors containing nitrogen as a heteroatoms; the resulting material is high-quality and poly-crystalline, with different doping percentages.

Finally, using a selected series of precursors, it is shown that the simultaneous presence of carbon, oxygen, and nitrogen behaves antagonistically to graphene's growth. The catalyst's surface changes its topography and the spontaneous growth of the material is inhibited.

KEYWORDS: graphene, growth, CVD, alcohols, heteroatoms, doping

RÉSUMÉ

LE RÔLE DE L'AZOTE, OXYGÈNE, ET CARBONE DANS LA CROISSANCE D'UNE LARGE MONO-COUCHE DE GRAPHÈNE SUR LE CATALYSEUR CUIVRE

Depuis son isolation en 2004 le graphène reste toujours un défi de synthèse pour les scientifiques. Afin de profiter du potentiel du graphène, des échantillons de haute qualité sont désirés, *i.e.* larges surfaces de graphène mono-crystallin. La synthèse par dépôt chimique en phase vapeur (CVD) est une des méthode de synthèse capable de satisfaire ces besoins. De plus, le dopage n de ce matériau ouvre sa gamme d'applications.

En utilisant des feuilles de cuivre comme catalyseur et différents précurseurs aliphatiques comme source de carbone, variables qualités de graphène peuvent être produites. Le méthane et l'acétylène restent les précurseurs les plus populaires. Dans ce travail il est montré que la synthèse à partir d'alcools aliphatiques (méthanol, éthanol, 1-propanol) est possible, et encore, que la présence de l'oxygène n'influence pas sur la qualité du matériau final. De plus, la modification du graphène par dopage est achevée en utilisant des précurseurs contenant l'azote comme hétéroatome; le résultat est du graphène de haute qualité, poly-crystallin, à différents pourcentages de dopage.

Enfin, en utilisant des précurseurs spécifiques il est montré que la présence simultanée du carbone, oxygène, et azote réagit de manière antagoniste à la croissance du graphène. La surface du catalyseur change de topographie et la croissance spontanée du matériau est inhibée.

MOTS CLÉS: graphene, croissance, CVD, alcools, hétéroatomes, dopage.

LIST OF ABBREVIATIONS, SYMBOLS, AND ACRONYMS

2D	Two dimensional
3D	Three dimensional
Å	Angstrom
AFM	Atomic Force Microscope
Au	Gold
C	Carbon
CNT	Carbon Nanotube
CO ₂	Carbon dioxide
CH ₄	Methane
CH ₃ NO ₂	Nitromethane
Co	Cobalt
Cr	Chrome
Cu	Copper
CuO	Cupric oxide, or copper(II) oxide
Cu ₂ O	Cuprous oxide, or copper(I) oxide
CVD	Chemical Vapor Deposition
DMF	Dimethylformamide
DNA	Deoxyribonucleic acid
EDA	Ethylenediamine
ESCA	Electron Spectroscopy for Chemical Analysis
H ₂	Hydrogen
H ₂ O	Water
Ir	Iridium
F	Fluorine
FeCl ₃	Ferric chloride, or iron(III) chloride
FWHM	Full-width at half-maximum

GaAs	Gallium Arsenide
M	Metal
Ni	Nickel
N ₂	Nitrogen
O ₂	Di-oxygen
Pd	Palladium
PDMS	Polydimethylsiloxane
PMMA	Polymethyl methacrylate
ppb	Parts per billion
Pt	Platinum
Re	Rhenium
Ru	Ruthenium
SEM	Scanning Electron Microscopy
Si	Silicon
SiC	Silicon Carbide
SiO ₂	Silicon Dioxide
sp ²	Trigonal atomic orbital hybridization
sp ³	Tetrahedral atomic orbital hybridization
T	Temperature in °C
TEM	Transmission Electron Microscopy
UV	Ultra-Violet
XPS	X-Ray Photoelectron Microscopy
ZnO	Zinc Oxide
π	Pi-bonding orbital

INTRODUCTION

0.1 Carbon Allotropes and Nanocarbons

Over 95% of our surrounding chemical environment is composed of “carbon compounds”. Organic chemistry forms the backbone of life. Among other elements which manage to bond with themselves in long chains, carbon is among the most versatile and strong. It can form single (bond energy of 350 kJ mol^{-1}), double (610 kJ mol^{-1}), and triple bonds (840 kJ mol^{-1}) with itself leading to a variety of structures and conformations useful in many fields of research. (Wudl, 2007) Historically, diamond and graphite were considered the main allotropic forms of carbon. Now, among them there are around a dozen forms. Amorphous carbon, obtained as a product of combustion from some materials, is composed of various ratios of sp^2/sp^3 hybridized carbons in no particular crystal arrangement. Other notable allotropes are fullerenes, nanotubes, carbynes, and the recently popular graphene.

Diamond is the hardest material known, with a hardness of 10 on the Mohs scale, and it's the thermodynamically stable form of carbon above 60 kbar of pressure. Its sought-after properties as well as its as-close-to-perfect-as-possible crystal structure receive numerous applications in science. It is a potent abrasive material, and it can be industrially synthesized. Diamond is composed of only sp^3 hybridized carbons, in which each carbon is covalently bonded to four other carbons. In conditions such as low pressures and under 1500°C diamond thermodynamically transforms into graphite. This conversion is very negligible in

ambient conditions.(Wudl, 2007)

Graphite can be pictured as a stacking of an infinite number of layers of sp^2 -hybridized carbon atoms; this layer is known as a graphene sheet. In such a layer each carbon atom is bonded to three others. This arrangement resembles the honeycombs of bees, a planar matrix of bonded hexagons. Each carbon has one unhybridized electron in the $2p_z$ orbital. The association of all these electrons forms delocalized π orbitals, assuring further stabilization for the in-plane bonds, much like scaffolds on both sides of a wall. Each layer has these delocalized orbitals on both sides, meaning that the stacking of the layers is based on $\pi - \pi$ interactions of Van der Waals nature. The layers are stacked together about 3.35 Å.(Chung, 2002)

The most common form of graphite stacking is the hexagonal *ABAB*; a less often version being the rhombohedral *ABCABC*. The various stacking arrangements and the weak Van der Waals interactions contribute to graphite's lubricant properties. Moreover, its electronic configuration gives it good planar (following the π bands and the σ bonds) conductive properties, of both electricity and heat; less so in the stacking direction due to Van der Waals interactions. An "imperfect" version is the turbostratic graphite, in which the inter-layer distance is variable due to a multitude of stacking faults (layer rotations or translations). Artificially, one can prepare well-ordered pyrolytic graphite through pyrolysis of a gas carbon source. Annealing this form of graphite produces highly oriented pyrolytic graphite with a mosaic spread of 0.02° and crystallites of around $1 \mu\text{m}$ in size.(Wudl, 2007)

The discovery of more exotic allotropic forms is a rather recent affair. Fullerenes

and nanotubes have been discovered and studied since the mid 1900's. Both materials form when the dangling bonds at the edges of a finite graphene layer bond together. The end product depends on the nature of the topological manipulations happening with graphene. The result has a lower material energy, but with increased bond strain.(Wudl, 2007)

Fullerenes are hollow spheres formed of various numbers of carbon atoms depending on shape and size, the most popular being C_{60} and C_{70} . The bond strain allows for facile functionalization opportunities of fullerenes. This has allowed scientists to take advantage of their properties in various fields, such as solar cells, and biological applications.(Wudl, 2007)

Carbon nanotubes also have their own merit due to their electric and mechanical properties. Depending on the folding axis of the graphene sheet, the resulting nanotube can behave either as a metal or a semi-conductor. Chemical functionalization is also relatively easy, allowing for applications in nanoelectronics, reinforcing in composite materials, biosensing, tissue engineering, drug delivery.(Wudl, 2007) Carbon onions are spherical concentric shells of graphene, or multi-walled fullerenes. One immediate application studied was the encapsulation of other materials for protective purposes.(Wudl, 2007)

Amorphous carbons have a longer history than their more exotic counterparts. They consist of roughly planar layers of sp^2 -hybridized carbons, with varying fractions of sp^3 carbons which provide crosslinking between neighbouring layers. These materials lack a well-defined crystallinity. These "soft carbons" can be prepared from the gas phase. Non-graphitizable carbons originate from solid precursors (polymers, resins) and have a high degree of disorder. They have isotropic properties, and their high degree of cross-linking do not allow for the formation

of graphitic structures. Activated carbons are part of the amorphous allotropes which have undergone chemical modifications. They are usually porous, with high surface areas ($500 \text{ m}^2 \text{ g}^{-1}$ to $3000 \text{ m}^2 \text{ g}^{-1}$). (Wudl, 2007)

0.2 Applications and Perspectives

The energy sector seems to be the most popular field in which carbon materials are used. Due to the versatility of its electronic structure through hybridization, carbon can form various structures. A series of processing routes allow scientists to take advantage of its versatility, obtaining modified versions, such as carbon fibers, carbon foams, meso-carbon-micro beads, and even carbon-carbon composites. (Srivastava *et al.*, 2009)

Graphite, the most common allotrope, has been used as a writing tool for hundreds of years. Its powder form has also proved to be a good dry lubricant, although that is due to the air trapped between the graphene layers. In vacuum the layers are subjected to Van der Waals interactions which make their separation quite difficult. (Wudl, 2007)

The delocalized π electrons in the graphene layers are responsible for graphite's in-plane conductivity. (Wudl, 2007) A mixture of carbon black (able to hold electrolytes) and graphite (conductive) is used in non-rechargeable batteries, and various carbon designs are used in rechargeable batteries: carbon fibers, carbon micro-beads, pitch coke, polymer-based carbons. (Srivastava *et al.*, 2009)

Some forms of carbon are known for their high H_2 absorbing capability. This has been exploited for applications in fuel cell technologies for parts such as catalyst supports, gas-diffusion systems, current-collector plates. Catalyst-filled carbon nano-tubes can be used as a membrane in fuel cells where they proved to be very effective in the reduction of oxygen and oxidation of methanol. (Srivastava *et al.*, 2009)

Hydrogen storage is another very attractive research subject. Its combustion produces energy and water vapours, with an energy density of 38 kW h kg^{-1} , almost 3 times that of gasoline. The cavities and micro-pores of carbon materials make them interesting candidates for hydrogen storage. However, it has been shown that CNT-derived materials have the highest potential due to their large external surface and the variable internal hollow cavity where gas can be stored by physisorption or chemisorption. (Srivastava *et al.*, 2009)

According to the study of Chesnokov *et al.* CNTs present a spring-like behaviour under 25 kbar of pressure. (Chesnokov *et al.*, 1999) This makes them promising candidates in composites for energy absorbing materials. (Srivastava *et al.*, 2009)

As far as electronic applications go, carbon allotropes have a rich potential. CNTs behave either as a metal or semi-conductor depending on their chirality – useful in flat panel displays, computer chips, cell phones, nano-circuitry. (Zhang *et al.*, 2007) Fullerenes seem useful in electronic textiles, molecular transistors, solar panels, and even electromagnetic interference shielding. (Srivastava *et al.*, 2009)

0.3 Conclusion

Carbon is a highly versatile element present everywhere around us, from it being the support of life to forming the hardest and strongest materials known to man. Its present and under-study applications cover a wide spectrum of fields which show considerable promise to improving human life.

CHAPTER I

CHARACTERIZATION METHODS

In this chapter a series of characterization techniques are presented. They are practical applications of matter-matter and energy-matter interactions phenomena.

1.1 Atomic Force Microscopy

Atomic Force Microscopy (AFM) was initially presented as an application of the “tunnelling effect” concept, allowing the surface study of electrically insulating materials. Combining tunnel effect microscopy and a profilometry stylus, Binnig, Quate, and Gerber showed that it is possible to get images of surfaces in ambient air, whether the material is conductive or not, with a resolution of 30 Å vertical, and 1 Å horizontal. (Quate, 1986) It has since been adapted to different environments: liquid, low temperatures, magnetic fields, and even optimized for biological and chemical applications.

The working principle is based on the measurement of the forces between the stylus and the analysed surface. The force is measured by a cantilever. Surface interactions modify the cantilever’s shape, these are observed by following the

reflection of a laser beam off its tip.

1.1.1 Microscope

A miniature tip on a cantilever approaches the sample surface. The sample is kept on a xy translation stage which moves it relative to the tip (Figure 1.1). An AFM tip can work in static or oscillating modes. (Frétigny, 2005)

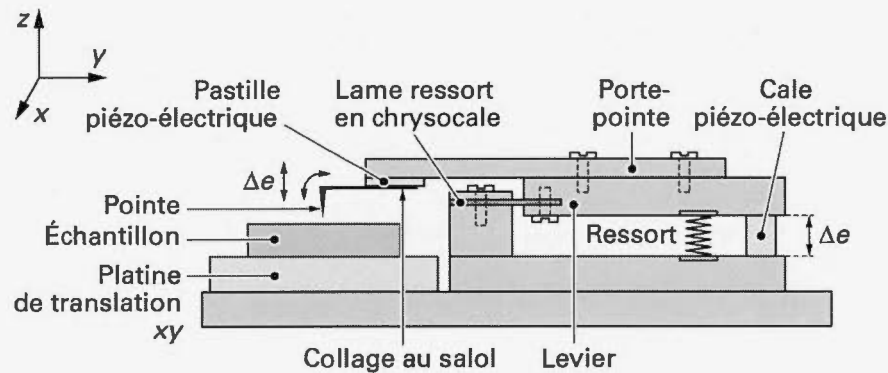


Figure 1.1: AFM cantilever and tip assembly schematic. (Frétigny, 2005)

There are three main operating modes on an AFM: static, dynamic, and thermal. The interactions can come from the Van der Waals forces between the tip and the sample, capillary forces, friction, and even magnetic processes. Chemically modifying the tip gives the opportunity to consult various surface properties of the sample.

Using a control loop it is possible to obtain “height” information of the surface (topography) by following a constant mechanical interaction; moreover, it also permits the measurement of viscoelasticity, tribological, and friction measurements. Another possibility is the measurement of distant forces between the surface and

the tip.(Frétigny, 2005)

1.1.2 Operating modes

Without vibrating the cantilever, the sample is brought closer to it (z axis) and the cantilever deflection is measured. One cycle is enough to obtain a force curve describing the sample-tip interaction. On approach, the interactions are weak, there is little to no deflection of the cantilever. In vacuum, air, liquids, this interaction is slightly attractive, phenomenon described by a negative cantilever deflection. Closing in even more, the deflection grows linearly with sample height. During retraction, the force curve carries the same shape as on approach, but surpasses the null force point; the adhesion forces are keeping the cantilever close to the surface. Once enough force is applied to release the tip the force curve resumes the same behaviour as on approach. This is resumed in Figure 1.2.

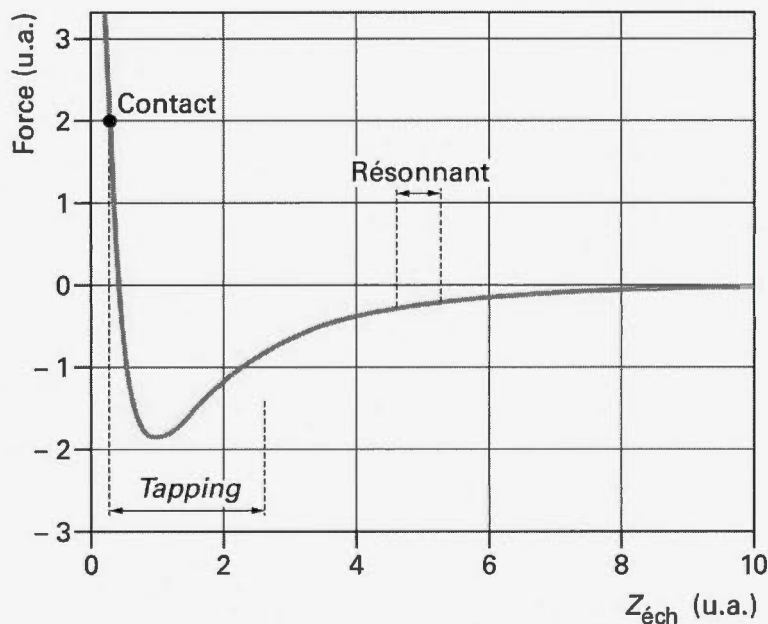


Figure 1.2: Surface-tip interaction curve.(Frétigny, 2005)

Contact mode

Following the force curve acquisition it is easy to continue into contact imaging mode; the deflection force of the probe is maintained constant, as the sample is translated on the x,y,z axis. The probe is in constant contact with the surface. This can, however, damage the surface of the sample, and reduce image quality. Nonetheless, it is a quick and easy method of imagery. It is often coupled with measurement of friction and adhesion forces, as well as contact stiffness (Young modulus).(Frétigny, 2005)

Resonance mode

The resonant mode uses the cantilever's natural resonance frequency. Far from the sample, and with a low amplitude, the cantilever oscillates. The force gradient depends on the tip position on the surface, and it causes a frequency displacement in the cantilever. Inversely, at a given oscillation frequency, the amplitude is modified and gives information on the local force gradient. This mode is seldom used in topography imagery, however it is useful in measuring long distance, electrical, and magnetic interactions.

Tapping mode

It is a non-linear resonance mode which consists of higher amplitudes and a shorter tip-sample distance than the resonance mode. With each cycle the tip gently "touches" the surface at a frequency close to the cantilever's resonance. The applied forces on the sample are significantly weak and the contact time is short, thus this mode is ideal for topographical imagery as the friction produced is insignificant. The sample is maintained intact, with little to no deformation or wear.

Moreover, the short contact time limits surface adhesion.

1.1.3 Other analysis

The AFM tips can be functionalized in order to study different materials' properties such as adhesion, chemical functionalization and specific chemical interactions, polymer elasticity. Generally, carbon nanotubes are used which provide a few-nanometers diameter tip useful for analysis.(Frétigny, 2005)

AFM is a highly versatile force measuring tool, capable of contact and distant forces measurement applicable in materials science, cellular biology, interface and surface studies, as well as indirect analysis through these methods.

1.2 X-Ray Photoelectron Spectroscopy

Atoms present at the surfaces of materials are the first responders to any interaction attempt with the bulk. The nature of these atoms dictates the types of interactions taking place: corrosion, catalysis, contact potential, adhesion. Therefore, surfaces influence a number of properties of the bulk. However, only a small number of these atoms are actually found on the surfaces. If we consider a 1 cm^3 cube, only an estimated 1 in 10^7 are present on a surface, giving roughly a concentration of 100 ppb. Obviously, this ratio depends on the morphology of the studied surfaces. In order to successfully analyse a surface, the technique used must be highly sensitive, and capable of filtering other interfering signals coming from impurities. One of the techniques used capable of satisfying surface analysis is X-ray Photoelectron Spectroscopy. This technique is effective at identifying surface elements, describing and quantifying their chemical states, giving a 3D distribution of elements, and even identifying if the surface is populated by thin

films.(Wolstenholme, 2003)

1.2.1 Electronic Spectroscopy

Electron spectroscopy is interested in the emission and analysis of low-energy electrons, usually 20 eV to 2000 eV. These electrons are emitted by the materials as a result of the photoelectric effect; Einstein's mathematical description of this phenomenon earned him a Nobel prize in Physics in 1921. Those electrons have a kinetic energy as such:

$$KE = h\mu - BE - \Phi_s \quad (1.1)$$

where $h\mu$ is the photon's energy, BE the binding energy of the originating atomic orbital, and Φ_s is the spectrometer's work function.(Moulder et al. 1992) These photoelectrons can be emitted from different shells, each at a specific energy and with different emission probabilities.

Electron-matter interaction happens more often than photon-matter, thus the electron mean free path is considerably smaller (tens of Angstroms) than photons' (micrometers). This means that the only electrons capable of leaving the bulk without energy loss are those present at depths inferior to tens of Angstroms. These electrons give the useful signals. The background is formed by electrons which have gone through energy loss processes. Useful electrons are then detected by an electron spectrometer according to kinetic energy.(Moulder *et al.*, 1992)

1.2.2 Interpretation

A general XPS spectra is a plot of electron binding energy versus the number of electrons counted in a specific energy interval. Well-defined peaks originate

from the electrons which haven't lost any energy while being ejected from the sample. The electrons are randomly collected in time, as a consequence the signals appear with some "noise" which isn't instrumental. The percent standard deviation for counts is indirectly proportional to the square root of the number of counts; the signal-to-noise ratio is proportional to the square root of the counting time. (Moulder *et al.*, 1992)

1.2.3 Identifying the chemical state

Properly characterizing a material by XPS first requires a good line identification. This can be made easier with proper instrumentation (voltage calibration, narrow sweep range). An immediate challenge is the static charge accumulation which needs correction. Insulating samples may acquire a steady-state charge during analysis. Positive charging is capable of shifting peaks to higher binding energies, while the opposite is applicable to negative charges. In order to overcome this obstacle there are a few steps which can be taken. The C1s position can be measured, known to appear at 284.6 eV; any shift from this value can be considered as a measure of the static charge. Trace quantities of Au can be evaporated on the sample; the Au4f doublet is recorded, then the analysis of interest is repeated. It is assumed that the potential of the gold islands reflects the surface charge of the sample. A simple correction can also be made with an internal standard. (Moulder *et al.*, 1992)

There are numerous factors concerning the proper interpretation of XPS chemical shifts, which is why peak assignment and data comparison is still done through cross referencing with literature.

Case of Carbon nanomaterials

The surface analysis potential of XPS is particularly useful in carbon materials studies due to the importance of surface structure and chemical composition which dictate the material's properties.

XPS spectra are able to provide information concerning the degree and nature of functionalization. Carbon nanomaterials have a highly versatile surface from a chemical point of view, supporting a large number of reactions. It is then important to clearly determine the chemical states of the elements at the surface. It is also known that C has several hybridization states, each with different characteristics which influence the material's behaviour. Graphite for instance is composed of mostly sp^2 bonded carbons (sp^3 being present at the edges). An XPS spectrum of this material should theoretically give a single peak of C1s around a binding energy of 284.2 eV. On the other hand diamond materials have a fully sp^3 bonding construction. The XPS signal of these materials should give a single peak around 286 eV. Following this information it is then easy to determine a ratio between the two kinds of hybridization by comparing the respective peaks. For instance the laser treatments of graphite produces diamond-like domains in the material. Higher the laser intensity, higher the sp^3 content. (Barron, 2011) Such an example can be seen in Figure 1.3.

In general, binding energy increases with decreasing electron density around the atom. Positive oxidation states register higher binding energies, in contrast with the reduced species which gain shielding, easing the electron expulsion.

As it was shown, XPS is a versatile technique in identifying the elemental composition of a material, as well as their the relative ratios. Furthermore, information such as hybridization, bonding, functionalization can be extracted from the data.

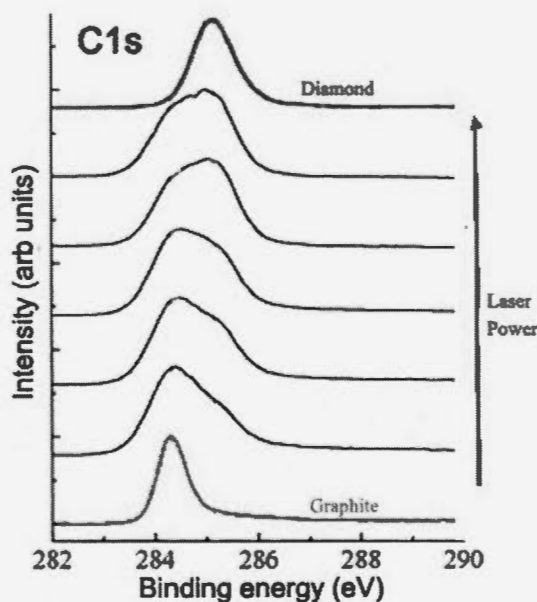


Figure 1.3: C1s high resolution XPS spectra of graphite, nanodiamond, and graphite with increasing laser power treatment. Adapted from Mérel et al. 1998.

This is a confident starting point in determining the carbon materials' properties, notably at the first atomic layers which are the most active.

1.3 Scanning Electron Microscopy and Transmission Electron Microscopy

In the early 20th century the electron's wave-particle duality was discovered. At a 50 V acceleration their wavelength reaches 0.17 nm. Such dimensions are comparable to atomic dimensions, making electrons useful in characterizing materials as they are strongly diffracted from the array of atoms on crystals' surface. At a 1000 times stronger acceleration (50 kV) their wavelength reaches 5 pm. These conditions allow a material penetration of up to several μm . In case of a crystalline solid the electrons are diffracted by the atomic planes. This is at the basis of transmission electron diffraction. Later, it was discovered that if these electrons could be focused the images obtained would have better spatial resolution than light-optical microscopes. Focusing electrons requires magnetic fields given

the particles' negative charge.(Egerton, 2005)

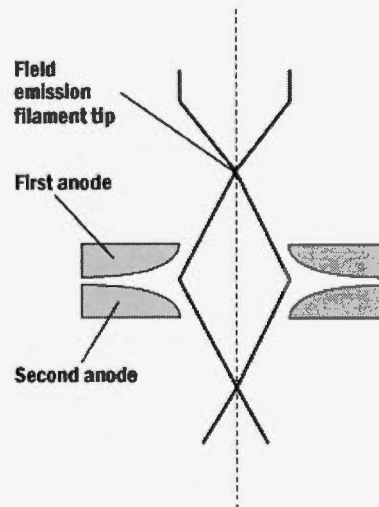


Figure 1.4: Electron beam source. Illustrated, a field emission filament tip cathode and the anodes responsible for the electron extraction.(of Iowa,)

1.3.1 Scanning Electron Microscopy

In SEM electrons are both elastically and non-elastically scattered when entering a solid. Some of them are elastically scattered at angles $>90^\circ$ with enough energy to leave the specimen and enter the vacuum – they are then collected as backscattered-electrons (BSE) and processed into a signal. Inelastic scattering involves low deflection angles, but it may reduce kinetic energy of the incident electrons until they are absorbed by the solid, and possibly become conduction electrons (in case of metals). The penetration depth increases with increasing acceleration energy.(Egerton, 2005)

1.3.2 Secondary Electron Imaging

Weakly bound electrons (mainly found in the outer shells) use only a small portion of the incident energy as means of escape from the atom's shell. The remaining energy is then kept as kinetic energy. These secondary electrons will eventually

non-elastically interfere with matter even before they escape the bulk. In doing so they lose kinetic energy, and only the ones originating near the surface are able to escape and be detected. The escape depth is generally $<2\text{ nm}$, thus images formed by secondary electrons (SEI) present a topographical contrast. There is almost always a contrast due to the fact that the secondary electron detector is positioned on the side of the column at an angle. The images are comparable to observing an object lighted on one side – brighter on the side more exposed to the light source. In the case of SEM the bright features are those facing the detector as the electrons originating from those zones have a higher probability of reaching the detector.(Egerton, 2005)

1.3.3 Backscattered Electron Imaging

Backscattered electrons are primary electrons scattered at angles $>90^\circ$ from the solid. Seeing how this interaction is elastic the energy of these electrons is similar to their initial acceleration. The backscattering coefficient depends strongly on the atomic number of the matter's composition. This gives elemental contrast images (Z dependant).(Egerton, 2005)

1.4 Raman

One of the most versatile and pertinent spectroscopy method used in this project is Raman spectroscopy, which has molecular vibrations as focus. The sample is excited by a laser at a set wavelength, and the scattered photons are recorded and analysed. The data extracted from them is capable of describing the vibrational state of the analyte.(Dent, 2005)

There are 3 sort of light scattering modes: Rayleigh diffusion which is simply the incident light elastically reflected at the same frequency as the incident light,

Stokes scattering which is diffused at a frequency lower than the incident light's (it subtracts the molecular vibration frequency), and anti-Stokes scattering at a higher frequency (it adds the molecular vibration frequency); these latter two compose Raman spectroscopy. Stokes lines are the most studied as their intensity is higher than anti-Stokes'.(Palsson, 2003)

1.4.1 Raman Fingerprint of some Carbon allotropes

Carbon is most abundantly present under its graphite form, among diamond, graphene, nanotubes, and fullerenes. The main allotropes studied are graphene and graphite.

Graphene

It is a 2D material, fully composed of sp^2 hybridized carbons. Its crystal lattice has a hexagonal symmetry ($D6h$), and its crystal structure has 2 atoms per lattice. For 2D structures Raman spectroscopy can give information on crystallite size, hybridization, presence of impurities, mass density, band gap energy, doping, defects and other crystalline disorders, number of graphene layers, carbon nanotube diameter, and even metallic versus semi-conductive behaviour.(Ferrari, 2007)

There are three main Raman bands for pristine graphene, G (1582 cm^{-1}), $2D$ (2500 cm^{-1} to 2800 cm^{-1}), and D (1345 cm^{-1}). The G peak originates from the elongation of the C–C bonds common to all the sp^2 hybridized systems. These bonds characteristics can be influenced (deformations, interactions with substrates or other interfaces) which in turn modify the hexagonal symmetry. For instance nanotubes' curves give a more complex G peak signal, while pristine graphene gives a single clear peak.(Ferrari *et al.*, 2006)

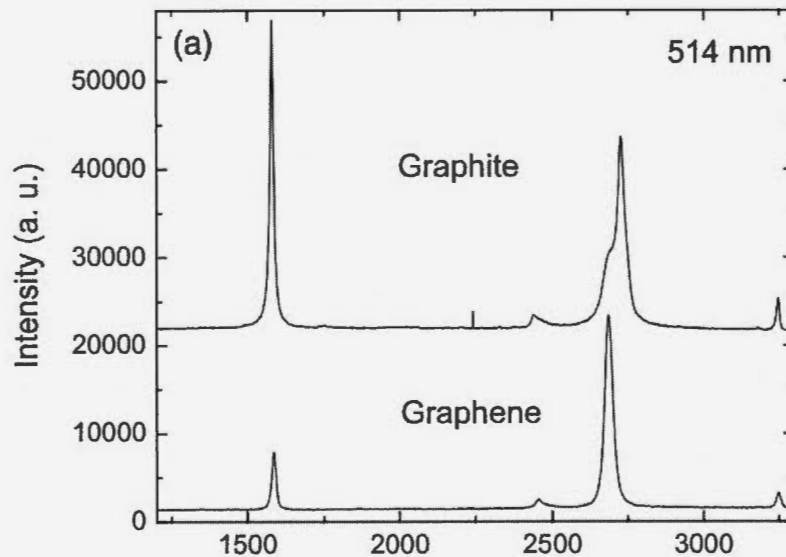


Figure 1.5: Comparison of Raman spectra at 514nm for bulk graphite and graphene; scaled to illustrate a similar height of the 2D peak around 2700 cm^{-1} .(Ferrari *et al.*, 2006)

The 2D band is a consequence from a phonon-phonon interaction, and it's dispersive, meaning the response signal depends on the excitation wavelength. This band can give information concerning graphene's electronic structure as well as its phonons, *i.e.* it is possible to differentiate mono, double, and several layered graphene, as well as its electronic structure. Practically, the 2D band has specific deconvolutions for graphene of 1 to 5 layers, above which the material's electronic structure begins to resemble graphite's and adopts that electronic and vibrational definition.(Ferrari *et al.*, 2006)

The last band of interest is the D band, known to appear from disorder in the sp^2 hybridized systems. These defects induce interesting resonance phenomenons. For instance it is possible to quantify the disorder in systems by comparing the 2D to G intensity ratios. Moreover if the ratio is lower than 0.5, then a single layer

of graphene is present, a ratio of 1 means that there are 2 layer, etc., however this quantification becomes difficult with increasing number of layers, as the effect on the intensity isn't linear. Another piece of information stems from doping induced resonance. Whenever a system is doped a D' peak appears which is an overtone band of the D band. Finally, several smaller peaks are present in a pristine graphene spectrum, however they are simply overtones.(Ferrari *et al.*, 2006)

Graphite

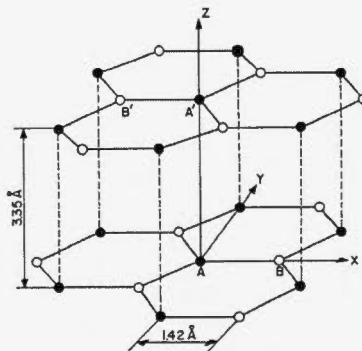


Figure 1.6: The crystal structure of graphite. Illustrated, its primitive unit cell, with dimensions $a = 2.46 \text{ \AA}$ and $c = 6.71 \text{ \AA}$, and an in-plane bond length of 1.42 \AA . A, A', B, and B' are the four atoms forming graphite's unit cell. Atoms A and A' (full circles) have neighbours directly above and below in adjacent layer planes; B and B' (open circles) have neighbours directly above and below in layer planes 6.71 \AA away.(Chung, 2002)

Graphite is simply put stacked graphene in an AB sequence. Its unit cell is composed of 4 atoms. This material has numerous vibrational modes, however only two are Raman active: the modes E_{2g1} and E_{2g2} . E_{2g2} is observed at around 1582 cm^{-1} , close to benzene's C-C vibration frequency. The second order harmonics of this mode is recorded at 3248 cm^{-1} . Less information is available for the E_{2g1} mode, although it has been measured to appear around 42 cm^{-1} . Inferior quality graphite presents a Raman peak at around 1355 cm^{-1} assignable to tetrahedral C bonds in a diamond structure.(Chung, 2002)

There are a few differences between graphite and graphene, as far as Raman spectroscopy goes. The $2D$ peak can be split in two elements for graphite: $2D_1$ and $2D_2$ with heights about $1/4$ and $1/2$ of the G peak respectively. It is also known that graphene's electronic structure evolves with increasing the number of layers. The $2D$ band has a single component for monolayer graphene, and reaches two components for the graphite. (Chung, 2002)

1.5 Conclusion

AFM, XPS, SEM, TEM, and Raman were covered, shown as versatile and complementary characterization techniques. All of them have been used during the study presented here.

CHAPTER II

GRAPHENE GROWTH FROM METHANE AND ALIPHATIC ALCOHOLS

2.1 Graphene, introduction

Since its isolation in 2004 by the Novoselov team the 2D material known as graphene has been the focus of several multi-disciplinary research subjects. Graphene is a material composed of sp^2 hybridized carbon atoms in a honeycomb lattice with a mono-atomic thickness estimated at around 8 \AA .(Dimitrakopoulos, 2012) It has been found that this material possesses various exceptional properties which stimulate the researcher's efforts in a large number of fields. Its crystal structure grants a particularly interesting band composition. Individual carbon atoms are separated by about 1.42 \AA from their 3 neighbours, constituting aromatic bonds in resonance.(Gray *et al.*, 2009) This gives rise to a zero band gap material acting as a semi-metal. As a consequence the charge carriers passing through it behave as Dirac fermions (zero effective mass), allowing them to ballistically travel up to 1 micron with mobilities of around $200\,000 \text{ cm}^2 \text{ V}^{-1} \text{ s}^{-1}$, a half-integer quantum Hall effect, all this while absorbing merely 2.3 % of visible light.(Lee, 2013) Among the most sought after applications are high frequency electronic devices, and transparent conductors. Its "miracle" characteristics have been observed while studying high quality samples, notably from mechanical exfoliation, and from its deposition on boron nitride. The alternative synthesis methods have yet to achieve these impressive characteristics.(Dimitrakopoulos, 2012)

2.2 Graphene synthesis methods

There are numerous methods of graphene and graphene-like structures production with various sizes, shapes, and quality, however only a few are industrially scalable. Among those we note liquid phase and thermal exfoliation, epitaxial growth on SiC, and Chemical Vapour Deposition.

2.2.1 Exfoliation

The exfoliation methods depart from graphite with the goal of separating the individual graphene flakes which compose it. The liquid method has two main paths, the first uses non-aqueous solvents with enough surface tension to favour an increase in the total area of the graphite crystallites, the second focuses on aqueous solutions of surfactants. Sonication, plus further treatment, aids the split of suspended monolayer flakes of graphene. A related route is the graphene oxide formation by oxidizing graphite crystallites, ultrasonically exfoliated, then processed. These methods allow the deposition of the material on almost any surface. Industrially it is more efficient to use a thermal shock procedure following the graphite's oxidation, which simultaneously achieves reduction and exfoliation.(Novoselov *et al.*, 2012) Moreover, it is possible to obtain graphene nanoribbons suspensions by carbon nanotube unzipping. These are more expensive methods, but can assure a tonne-level of production of well-defined distributions of graphene. Research is under way to use these methods in creating graphene-based inks, paints, electronics, electromagnetic shielding, barrier coatings etc.(Novoselov *et al.*, 2012)

2.2.2 SiC epitaxy

It has been demonstrated that graphitic layers can be grown on both faces of a SiC wafer by sublimating Si atoms leaving behind graphitized carbon. This method yields very high quality graphene with domains capable of reaching hundreds of microns in size. Despite its attraction this method has several drawbacks. SiC wafers are costly, and the temperatures required for the sublimation go beyond 1000 °C. Moreover, the SiC surface's required homogeneity is high – dangling bonds, if present, are able to bind covalently with graphene, thus rendering the first layer unusable.(Riedl *et al.*, 2010) Nonetheless, SiC graphene has some niche applications such as high frequency transistors, short-gate transistors, and even in metrological resistance standards.(Novoselov *et al.*, 2012)

It is apparent that the high temperature issue remains the most important. Moreover, future work should address the other problems such as elimination of terraces, the growth of multi-layer graphene at the edge of terraces, unintentional doping from the substrate and buffer layers, as well as increasing the crystallites size.(Novoselov *et al.*, 2012)

2.3 Chemical Vapour Deposition graphene growth

Chemical vapour deposition (CVD) is one of the methods capable of producing large-area, uniform, polycrystalline graphene films.

2.3.1 Chemical Vapour Deposition systems

As its name implies, the CVD system involves the use of vapours from various sources, either gas, liquid (evaporation), or solid (sublimation). The vapour flow is generally measured by mass-flow controllers. Vapours are then passed through high-temperature resistant tubes of quartz, ceramic, or stainless steel. The vapour circulation is assured by a vacuum system, and the pressure measured by thermocouple and ion gauges for higher vacuum. The vacuum, depending on the use, is provided by a simple mechanical pump, or by more powerful combinations of diffusion with mechanical pumps, as in our case (Figure 2.1), or by a turbo-molecular pump.

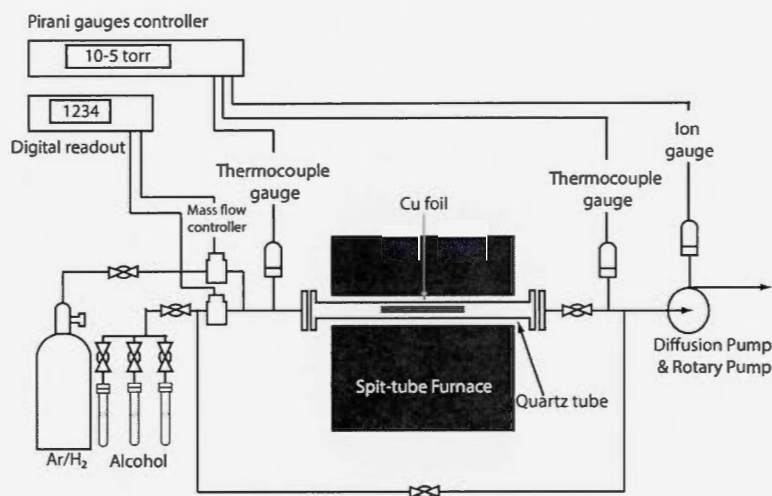


Figure 2.1: Schematic representation of the used CVD system. (Guermoune *et al.*, 2011).

2.3.2 CVD graphene growth process

The formation of few layer graphene on transition metal surfaces (Re, (Miniussi *et al.*, 2011) Ru, (P. W. Sutter, Flege, and Sutter 2008) Ir, (Coraux *et al.* 2008)

Co,(Ago et al. 2010) Ni,(Kim et al. 2009) Pt,(Sutter *et al.*, 2009) Pd(Kwon *et al.*, 2009)) has been demonstrated in the past few years. The deposition mechanism depends on the growth conditions and carbon solubility. Results of growth on inexpensive polycrystalline Ni and Cu substrates have stimulated the interest in using CVD for large area depositions. Copper proves to be the most efficient catalyst as far as price, handling, and quality of graphene go. Over 95 % of the copper surface is covered by single layer graphene, the rest being multilayer.(Li *et al.*, 2009a) Graphene growth on copper involves the thermal decomposition of a carbon source at high temperature. Gas, liquid, and solid precursors such as acetylene,(Nandamuri *et al.*, 2010) methane,(Li *et al.*, 2009a) hexane,(Mendoza, 2011) alcohols,(Guermoune *et al.*, 2011) and polymers(Byun *et al.*, 2011) can be used. Another important factor is the catalyst pre-treatment. As-received copper substrates are covered by native oxides (CuO, Cu₂O) which may diminish copper's catalytic activity. Two steps have been proven to remove these oxides. First a wet chemical pre-treatment by dipping in acetic acid, then an annealing treatment at 1000 °C. Besides oxide removal, the annealing increases the Cu grain size and modifies its morphology, which has been shown to have an effect on the size and quality of the graphene domains.(Han *et al.*, 2011)

The growth mechanism starts from nucleation sites from which flakes of graphene grow. With time the graphene domains increase in size, and eventually coalesce into one continuous layer. It has been shown that by tuning the pre-treatment conditions, partial pressure of the carbon source, and total growth pressure the nucleation density and flake size can be controlled. After the growth of a continuous sheet of graphene further exposure to the growth conditions does not lead to the formation of multiple layers of graphene. It has, however, been shown that the precursor feed rate can have a significant influence on the quality of the obtained

graphene.(Cui *et al.*, 2012)

The growth mechanism is a surface phenomenon, and not related to diffusion from bulk. This has been illustrated by the Ruoff group while growing graphene with a sequence of $^{13}\text{CH}_4$ and $^{12}\text{CH}_4$ (Figure 2.2). The Raman signatures of the two carbons differ slightly, which in turn translates into well differentiated Raman maps illustrating the regions in which ^{12}C and ^{13}C were sequentially used as precursors.(Li *et al.*, 2009b)

The as-grown layer of graphene contains wrinkles, explainable by the difference in the thermal expansion coefficients of the catalyst and graphene ($\alpha_{\text{graphene}} = -6 \times 10^{-6} \text{ K}^{-1}$ at 27°C , $\alpha_{\text{graphite}} = 0.9 \times 10^{-6} \text{ K}^{-1}$ between 600°C to 800°C , $\alpha_{\text{Cu}} = 24 \times 10^{-6} \text{ K}^{-1}$). These values suggest that graphene shrinks significantly with Cu cooling, generating mechanical stress, and its release is translated into the formation of wrinkles.(Mattevi *et al.*, 2011)

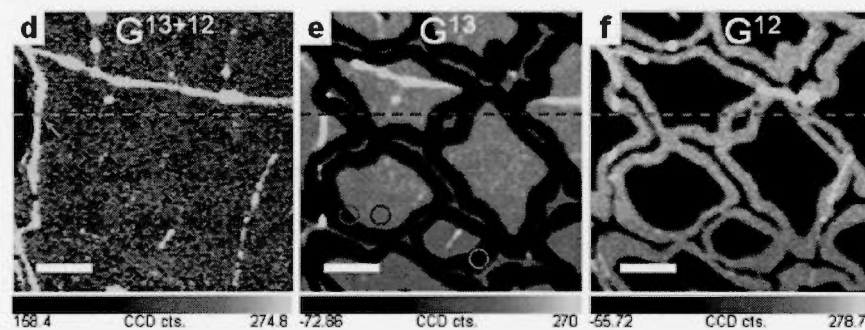


Figure 2.2: Micro-Raman characterization of the isotope-labeled graphene grown on Cu foil and transferred onto a SiO_2/Si wafer. Integrated intensity Raman maps of (d) G_{13+12} (1500 cm^{-1} to 1620 cm^{-1}), (e) G_{13} (1500 cm^{-1} to 1560 cm^{-1}), and (f) G_{12} (1560 cm^{-1} to 1620 cm^{-1}). Scale bars are $5 \mu\text{m}$.(Li *et al.*, 2009b)

Besides spectroscopy, the quality of the graphene films can be characterized by

measuring its carrier mobility, optical transparency, and sheet conductance. (Cooper *et al.*, 2012) In order to perform those measurements the film must be transferred onto other substrates. This is usually done by first depositing a polymer coating on the graphene film, typically PDMS or PMMA, then etching the underlying copper in a FeCl_3 or $(\text{NH}_4)_2\text{S}_2\text{O}_8$ (ammonium persulfate) solution. This last step is performed by immersing the graphene bearing substrate on the etching bath until a free-standing polymer/graphene membrane is observed floating on the bath. The transfer step has been proven to cause damage to the graphene film. (Kang *et al.*, 2012) In order to minimize the film cracking it is important to promote a high adhesion between graphene and the target substrate. Roughness and hydrophobicity are the main factors influencing graphene's adhesion. (Martins *et al.*, 2013)

The transfer procedure exposes the graphene to various chemicals and to certain degrees of mechanical stress. These factors participate in producing or enhancing structural defects in graphene, (Kang *et al.*, 2012) as well as possibly introducing undesirable impurities.

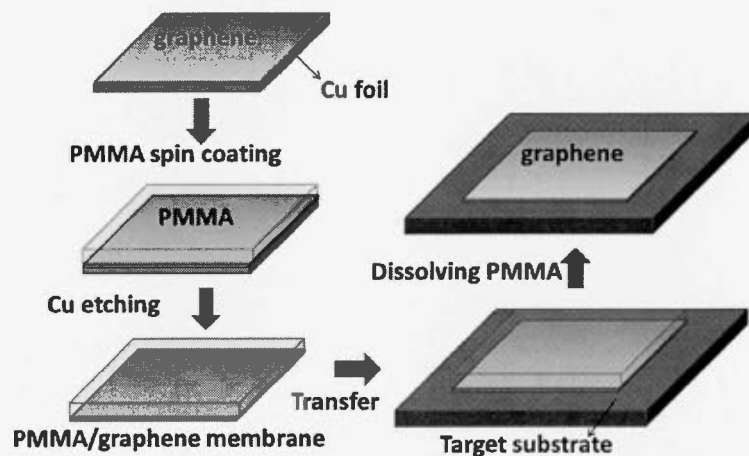


Figure 2.3: Schematic representation of the transfer procedure of graphene grown on copper foils. (Lee, 2013)

So far its properties have been maintained at a satisfactory level. Reported mobilities vary between $700 \text{ cm}^2 \text{ V}^{-1} \text{ s}^{-1}$ to $3000 \text{ cm}^2 \text{ V}^{-1} \text{ s}^{-1}$. The best optoelectronic properties have so far been obtained by Bae *et al.* 2010 with a Hall mobility of $5100 \text{ cm}^2 \text{ V}^{-1} \text{ s}^{-1}$ and a sheet resistance of 30Ω at 90 % transmittance.(Mattevi *et al.*, 2011)

2.4 Synthesis from alcohols

Single-layer graphene was synthesized from ethanol on Ni foils in an Ar atmosphere under atmospheric pressure by flash cooling after chemical vapor deposition, but a wide variation in graphene layer number was measured over the metal surface.(Miyata *et al.*, 2010) The same observation has been made when graphene was grown from ethanol and pentane under atmospheric pressure.(Dong *et al.*, 2011) Ethanol was also used to produce graphene by CVD on commercial stainless steel; however, the type of elemental species present in stainless steel is inhomogeneous, causing graphene growth to be enhanced in some areas and retarded in others.(John *et al.*, 2011) Moreover, single and few-layer graphene films were grown employing a vacuum assisted, CVD technique on Cu foils using liquid n-hexane precursor.(Srivastava *et al.*, 2010) At a very low growth temperature of 300°C with benzene as a precursor, small flakes of graphene were grown.(Li *et al.*, 2011) Copper appears to have a low oxygen affinity which allows graphene growth even if the source of carbon is a solid, such as sugar.(Sun *et al.*, 2010)

CVD growth of large-area, high quality graphene on Cu foils using aliphatic alcohols (methanol, ethanol, and 1-propanol) as carbon sources has been achieved. Copper is the favoured transition metal because its low carbon solubility leads to easier control of graphene growth by surface adsorption, rather than dissolution,

segregation and precipitation, as it takes place in nickel.(Li *et al.*, 2009a) Alcohols such as methanol, ethanol and 1-propanol are comparatively cheaper, easier to use, and less flammable than high purity methane and thus advantageous as liquid precursors for graphene growth. A detailed analysis of the CVD grown graphene layers was performed, including Raman spectroscopy, Raman mapping, scanning electron microscopy (SEM), optical imaging, X-ray photoemission spectroscopy (XPS) and a comparison to graphene produced by methane decomposition.(Guermoune *et al.*, 2011)

2.4.1 Experimental procedure

Graphene growth begins by cleaning the Cu catalysts. Twenty-five micrometer thick, Cu foils (Alfa Aesar, N# 13382) are immersed in 1 M acetic acid at 60 °C for 10 minutes followed by immersion in acetone and 2-propanol for 10 minutes in each solvent. The Cu foils are then loaded into a quartz tube and exposed to a 10 sccm, 10 mTorr environment of H₂ while the temperature is raised to its optimal value of 850 °C. The quartz tube is then held at this temperature for 20 minutes to remove any generated oxide or oxide layers on the Cu. Alcohols were outgassed to 10×10^{-6} Torr using several freeze-pump-thaw cycles. Upon introduction of the alcohol vapor to the system, the tube pressure increases to 1 Torr, a pressure below the saturated vapour pressure of all three alcohols at room temperature, thus allowing the vapours to be drawn into the chamber.

The Cu films are exposed to the alcohol vapours for approximately 5 minutes at 1 Torr. Next, the flow is cut off and the system rapidly cooled to room temperature with rates varying from 300 °C min⁻¹ to 30 °C min⁻¹ while maintaining the H₂ pressure at 10 mTorr. After growth, poly(methyl methacrylate) (PMMA,

950 kDa, 4% solution in anisole) is spin coated onto the surface of the graphene coated Cu. A hard bake at 120 °C for 1 minute is performed to stiffen the PMMA handle. The sample is subsequently immersed in a room temperature ammonium persulfate (0.1 M) bath to etch the Cu foil. The remaining PMMA-supported graphene is carefully transferred on a de-ionized water bath to remove residual etchant. The target substrate is used to lift the PMMA-supported graphene from the water bath (Figure 2.3). Heavily n-doped Si with 300 nm of dry, chlorinated thermal oxide, was chosen as the substrate. The sample is then dried at ambient temperature for 48h in a clean environment. Liquid PMMA is drop cast on the stiffened PMMA handle to release tension and promote conformal adhesion to the substrate. It is then dissolved in a warm acetone bath to produce a pristine graphene layer on the target substrate.

2.4.2 Characterization

The qualities were compared of CVD grown graphene with alcohol precursors to methane gas source.

X-Ray Photoelectron Spectroscopy

High definition C1s XPS data for the produced graphene films are presented in Figure 2.4. The data for the alcohol based graphene grown at 850 °C is compared to the pristine methane sourced films. Monolayer graphene displays a single peak around 284.5 eV. The lack of a shoulder between 286 eV to 287 eV indicates that the oxygen moieties present in the precursors have no measurable effect, doping or oxidation, on the resulting graphene layer.

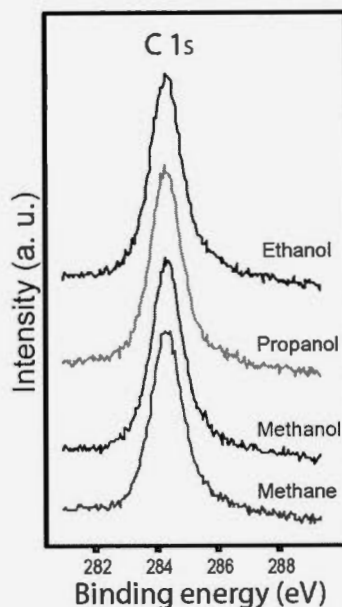


Figure 2.4: C1s XPS data for alcohol and methane grown graphene. No oxygen-doped peak was observed for pristine graphene.

SEM and optical imagery

The SEM images present homogenous and uniform films from alcohols and methane. Alcohol grown graphene was successfully transferred onto SiO_2/Si substrates, producing samples of size comparable to our quartz furnace tube's diameter, $3 \times 3 \text{ cm}^2$. Optical microscopy supports the cleanliness and continuity of the transferred graphene layers, as shown in Figure 2.6.

Raman Spectroscopy

Raman spectroscopy (Renishaw inVia) with a 514.5 nm pump laser was used to characterize the thickness and quality of the methane and alcohol grown graphene. Figure 2.7 shows the measured Raman spectra of graphene produced with methane and alcohol precursors, obtained after transfer on SiO_2/Si substrates. From the Raman spectra, graphene synthesized from alcohol precursors is of comparable

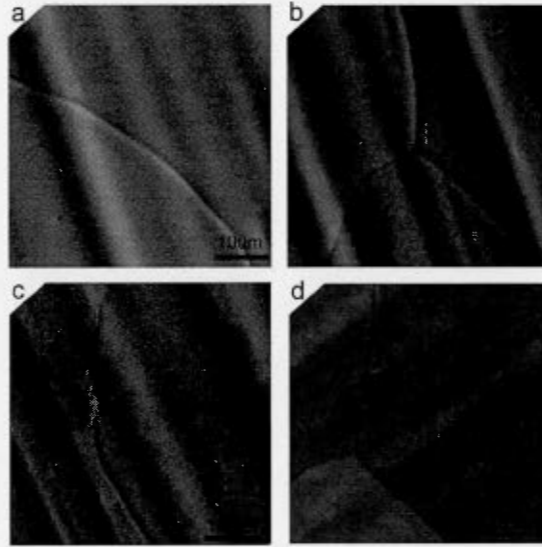


Figure 2.5: SEM images of graphene on 25 μm Cu foil substrates, compared for growth by (a) methanol (b) ethanol (c) 1-propanol and (d) gas source methane. The images show the presence of Cu surface steps, and graphene wrinkles which result from the difference between the thermal expansion coefficient of graphene and Cu, indicating that the graphene film is continuous and uniform.

quality to graphene synthesized by methane. The methane Raman spectrum has a large, symmetrical G peak and $2D$ peak at 1580 cm^{-1} and 2700 cm^{-1} , respectively. Moreover, the integrated intensity I_{2D} of the $2D$ peak is at least twice as large as the integrated intensity I_G of the G peak in most of the sample area. This indicates that uniform, large-area monolayer graphene has been grown. (Ferrari *et al.*, 2006) The $2D$ band is characterized by a single, sharp Lorentzian peak with a full width, half maximum (FWHM) of 30 cm^{-1} to 35 cm^{-1} , a result which correlates with graphene grown on SiC and transferred onto SiO_2 , (Lee *et al.*, 2008) on metal films by CVD (Li *et al.*, 2009a, Malard *et al.*, 2009, Reina *et al.*, 2009, Yan *et al.*, 2011, Lee *et al.*, 2010) and graphene layers on dielectric surfaces. (Ismach *et al.*, 2010) The comparatively small, integrated intensity I_D of the D -band peaks indicates a low defect density. The crystal domain size was estimated according

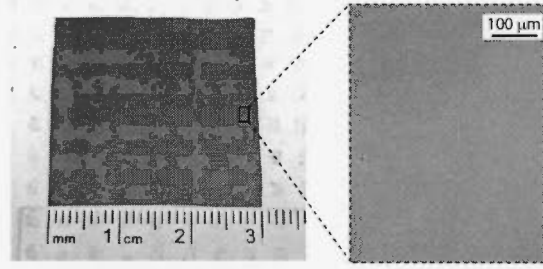


Figure 2.6: A $3 \times 3 \text{ cm}^2$ CVD graphene film grown using methanol, transferred to a SiO_2/Si substrate.

to the D/G peaks intensities ratio,

$$L_\alpha(\text{nm}) = 2.4 \times 10^{-10} \lambda_{laser}^4 \left(\frac{I_G}{I_D} \right) \quad (2.1)$$

where λ_{laser} is the laser wavelength (in nm). (Pimenta *et al.*, 2007) Representative crystal domain sizes are L_α 672, 130, and 168 nm for the methanol, propanol and ethanol grown graphene films, respectively. Figure 2.5 displays scanning electron microscopy (SEM) images of graphene as grown on Cu foil catalysts. Cu surface steps are visible as are graphene wrinkles resulting from the difference in the coefficient of thermal expansion between graphene and Cu. This is indicative of graphene continuity, since these wrinkles span the Cu grain boundaries. (Li *et al.*, 2009a)

By extracting characteristic features of the band structure for different graphene layers through Raman spectroscopy, we can distinguish easily between one layer graphene and few layer graphene (graphite). (Thomsen, 2004) The Raman fingerprint for single-layer graphene is related directly to the position and $2D$ -peak width. (Ferrari *et al.*, 2006, Lee *et al.*, 2008, Malard *et al.*, 2009, Reina *et al.*, 2009, Yan *et al.*, 2011, Lee *et al.*, 2010, Ismach *et al.*, 2010) A narrow and intense Lorentzian $2D$ -peak at 2700 cm^{-1} is a direct signature of single-layer graphene, while broadening and blue-shifting of the $2D$ -peak (with multiple Lorentzian line-

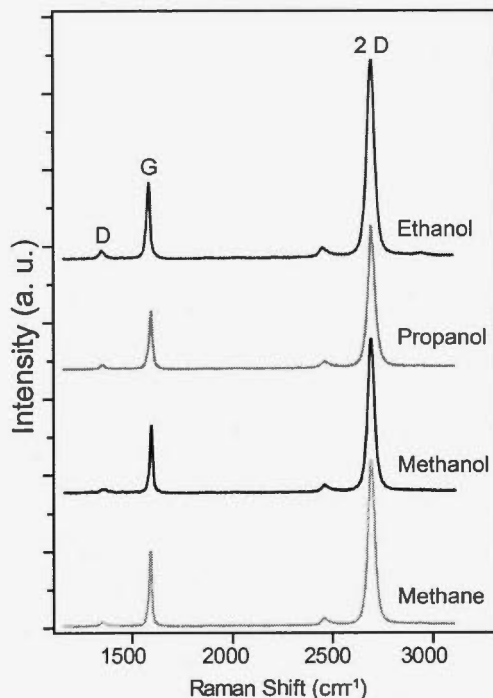


Figure 2.7: Raman spectra of a transferred CVD graphene film on SiO_2/Si compared for growth by methanol, ethanol and 1-propanol. The small D peak (1350 cm^{-1}) and the intensity of the $2D$ peak (2700 cm^{-1}) found to be more than twice as high as the G peak (1580 cm^{-1}) indicate the presence of high quality monolayer graphene.

shapes) indicates multiple graphene layers.

The effect of furnace temperature during growth upon the quality of the transferred graphene was investigated systematically with Raman spectroscopy for methanol, ethanol and 1-propanol precursors (Figure 2.8). As growth temperature was increased from 650°C to 850°C , the $2D$ peak sharpened and the intensity of the D peak (1350 cm^{-1}) decreased (Figure 2.8A), indicating an increase in graphene crystal domain size and thus improved graphene quality with increasing growth temperature (Figure 2.8C). A sharp, single Lorentzian $2D$ peak at 2700 cm^{-1} is evident in graphene samples grown at 850°C .(Ferrari *et al.*,

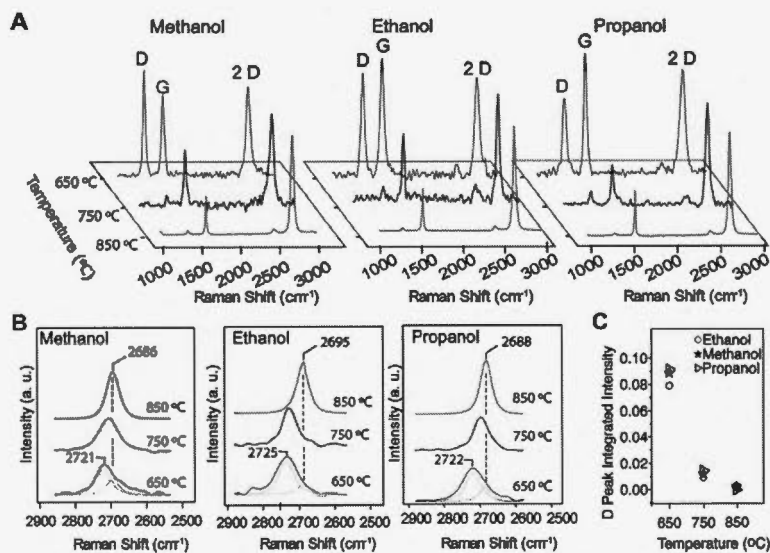


Figure 2.8: Raman spectra of transferred CVD graphene compared by precursor and growth temperature. A Renishaw inVia spectrometer, 514.5 nm laser wavelength, and 100x objective lens was used. (A) With a temperature increase from 650 °C to 850 °C, the intensity of the *D* peak (1350 cm⁻¹) decreases and the 2*D* peak sharpens, indicating a reduction in defect density and improved graphene quality. (B) Evolution of the *D* band with temperature, noting the fit of two Lorentzians (650 °C) turning into one at 850 °C, characteristic of monolayer graphene. (C) No significant difference is observed in *D* peak integrated intensity versus alcohol precursor.

2006) A growth temperature of 850 °C was thus selected for high-quality alcohol grown graphene. The variations of *D*-peak (1350 cm⁻¹) intensity, with respect to temperature, for each alcohol are plotted in Figure 2.8C. The decrease in the *D* peak intensity correlates with the increase in temperature, implying that there is little disorder in graphene films grown at 850 °C. Analysis of the 2*D*-peak of synthesized graphene at growth temperatures 650 °C and 750 °C indicates a doublet at 2700 cm⁻¹ and 2730 cm⁻¹ (Figure 2.8B). For all alcohols, the Raman spectra at 750 °C show a majority component at 2730 cm⁻¹ and a minority component at 2700 cm⁻¹. In contrast to the Raman spectra of a mechanically exfoliated graphene monolayer and methane CVD graphene, where a single 2*D* peak at 2700 cm⁻¹ is observed, 2*D* peaks at 2700 cm⁻¹ and 2730 cm⁻¹ can be

readily assigned to monolayer and few layers graphene,(Ferrari *et al.*, 2006) respectively. However, at 850 °C, as monitored by a single Lorentzian profile $2D$ peak at 2700 cm^{-1} , the decomposition of alcohols leads to monolayer graphene formation.

2.5 Conclusion

A simple and effective method was shown, to synthesize graphene on Cu using easy to handle liquid alcohols: methanol, ethanol and 1-propanol. This method is an improvement to methane-based graphene growth since it is cheaper and safer, thus making graphene fabrication more accessible. Using the large scale characterization metrics presented, there is no apparent difference between graphene grown by a high purity carbon source (such as methane) and an oxygen rich carbon source (such as alcohols). This novel synthesis route suggests that further investigation is warranted for the study of new precursors based on liquid organic solvents in lieu of high purity gaseous hydrocarbons.

CHAPTER III

N-GRAPHENE GROWTH FROM NITROGEN CONTAINING PRECURSORS

3.1 Doped graphene

As remarkable as pristine graphene can be, it is desirable to control its electrical properties. One of the ways in which this can be achieved is by electron acceptor (p) or donor (n) doping. For example, the field effect behavior of graphene devices can be changed significantly by covalent edge doping and trace molecular gas adsorption. (Jin *et al.*, 2011) Theoretical studies have shown that by substituting carbon with nitrogen in graphene's crystal lattice results in a modulation of its properties towards an n -type semiconductor. Moreover, boron substitution can create a p -type semiconductor. The resulting electron and hole transport features were found to be asymmetric with respect to the Dirac point. (Lherbier *et al.*, 2008) So far, few-layer n -doped graphene has been synthesized by the arc discharge method, (Panchokarla *et al.*, 2009) using the CVD method with ammonia precursor (Wei *et al.*, 2009, Qu *et al.*, 2010) among others. Large surface, monolayer n -doped graphene has proven to be more difficult to achieve, however the Tour team has managed to synthesize it by CVD using pyridine as the precursor, assuring the presence of both C and N. (Jin *et al.*, 2011) Later, the same method was used with dimethylformamide (DMF), an inexpensive and common organic solvent. (Gao *et al.*, 2012) A doping percentage of 3.4% was achieved. As the research continues and the quality of the material advances it will be possible

to use it in applications such as fuel cell electrocatalysis, field effect transistors, lithium-ion batteries, ultracapacitors, electro- and biochemical sensing, quantum dots anchor in photocatalysis, etc.(Wang *et al.*, 2012)

The *p*-type doping of graphene has been performed extensively through physisorption. Aromatic molecules such as 9,10-Dibromo-anthracene, 1,3,6,8-pyrenetetrasulfonic acid, among others, attach to the surface of graphene, and their electronic structures influence that of graphene's.(Dong *et al.*, 2009) This approach is inspired by the similar studies done on carbon nanotubes,(Shin *et al.*, 2008) adding donor or acceptor sites by varying the functional groups of the physisorbed molecules. A more secure way of achieving the same, or similar results, is analogous to *n*-doping, which is to replace the carbon atoms with hole-creating species, such as boron and phosphorous. Phosphorous doping has been achieved on reduced graphene oxide following an annealing treatment with 1-butyl-3-methylimidazolium hexafluorophosphate, showing up to 1.16% doping.(Li *et al.*, 2013) Boron doping, however, has been studied through a CVD reaction with boric acid, obtaining up to 4.3% doping.(Wu *et al.*, 2012)

For the present work the doping of graphene has been attempted with a series of precursors, notably pyridine, dimethylformamide, ethylenediamine, and even N-methylimidazole. The CVD growth conditions are almost similar to those from alcohols or methane; the required pressure for these precursors is around 10 Torr for a 30 minute reaction time at 1000 °C. However, the road towards finding those conditions started by performing reactions in familiar conditions - starting from 500 mTorr, but characterization of the product did not reveal the formation of a graphene film.

The study was conducted with the aforementioned precursors for a growth time of

30 minutes under 10 Torr of H₂ pressure, and a precursor partial pressure of around 4×10^{-4} Torr calibrated with a high precision valve. Raman characterization was then performed on samples which were transferred on SiO₂/Si substrates.

3.2 Characterization and discussion

3.2.1 XPS

The incorporation of nitrogen into the graphene lattice is supported by XPS analysis (Figure 3.1 and Figure 3.2), where graphene grown from ethylenediamine, N-methylimidazole, pyridine, and dimethylformamide show an XPS peak at the N 1s binding energy around 400 eV, indicative of nitrogen in a modified carbon crystal lattice. (Lin *et al.*, 2010, Point *et al.*, 2005, Ronning *et al.*, 1998, Marton *et al.*, 1994, Pels *et al.*, 1995) The C1s core-level is observed at 284.8 eV and (285.8 ± 0.3) eV, corresponding to graphitic carbon-carbon sp^2 hybridization and the carbon-nitrogen double bond (C=N) respectively. (Ronning *et al.*, 1998, Marton *et al.*, 1994) A minor line at (288.0 ± 0.3) eV is most likely due to C–O bonds from oxygen surface contamination. (Moulder *et al.*, 1992) The N1s peak from pyridine (Figure 3.2a) and N-methylimidazole (Figure 3.1b) grown N-graphene are fitted with components centered at 398.9 eV and (400.5 ± 0.2) eV, corresponding to pyridinic and pyrrolic forms (Marton *et al.*, 1994, Pels *et al.*, 1995) where nitrogen has two carbon neighbors in either a hexagonal or pentagonal ring configuration, respectively. The same binding energies were observed for ethylenediamine with an additional component at 401.5 eV corresponding to graphitic nitrogen (Figure 3.1a) wherein nitrogen is bonded to three carbons. (Marton *et al.*, 1994, Pels *et al.*, 1995) Our XPS analysis suggests that the predominant nitrogen configuration in graphene grown with pyridine and N-methylimidazole precursors is a mixture of pyridinic and pyrrolic moieties. The family of nitrogen moieties is extended to include the graphitic form with ethylenediamine precursor growths,

with a corresponding FWHM of the N1s peak that is much broader. The change in nitrogen incorporation may be due to the precursor's structure. Ethylenediamine contains nitrogen bound to carbon in an sp^3 configuration while pyridine and N-methylimidazole contain nitrogen in imine or sp^2 form. The imine form and its related configuration reported by different groups seems influenced directly by N-graphene CVD growth conditions. (Meyer *et al.*, 2011, Luo *et al.*, 2011, Zhang *et al.*, 2011, Sun *et al.*, 2010, Jin *et al.*, 2011, Saiki, 2011, Usachov *et al.*, 2011)

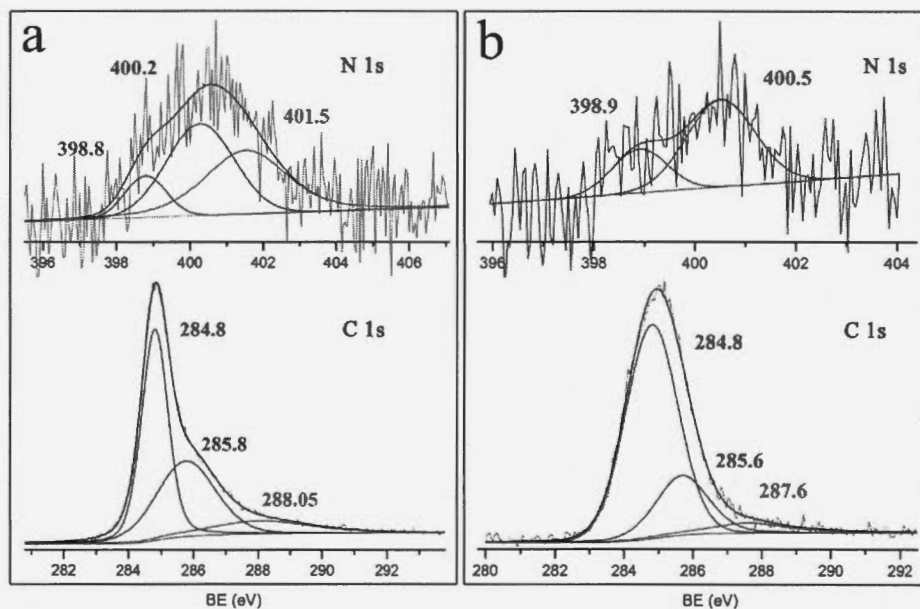


Figure 3.1: XPS characterization of N-doped graphene grown up to 30 minutes. C1s and N1s core-level X-ray photoelectron spectra of grown graphene from : a) ethylenediamine b) N-methylimidazole. The C1s peak can be split to three Lorentzian peaks labeled by red, blue, and green lines corresponding to graphite-like sp^2 C, N_{sp^2} -C bond and CO (due to absorbed oxygen) respectively. The N1s peak can be split to Lorentzian corresponding to pyridinic, pyrrolic and graphitic forms labeled by red, blue and green lines respectively.

Graphene grown from dimethylformamide exhibits a poor signal to noise ratio in the N1s spectrum due to a low nitrogen content, prohibiting any meaningful spectral analysis (Figure 3.2b). As has been previously shown, graphene grown

on copper has a very low affinity for oxygen, (Guermoune *et al.*, 2011) suggesting that the oxygen within the dimethylformamide molecule is able to prevent nitrogen incorporation into graphene during the CVD growth process.

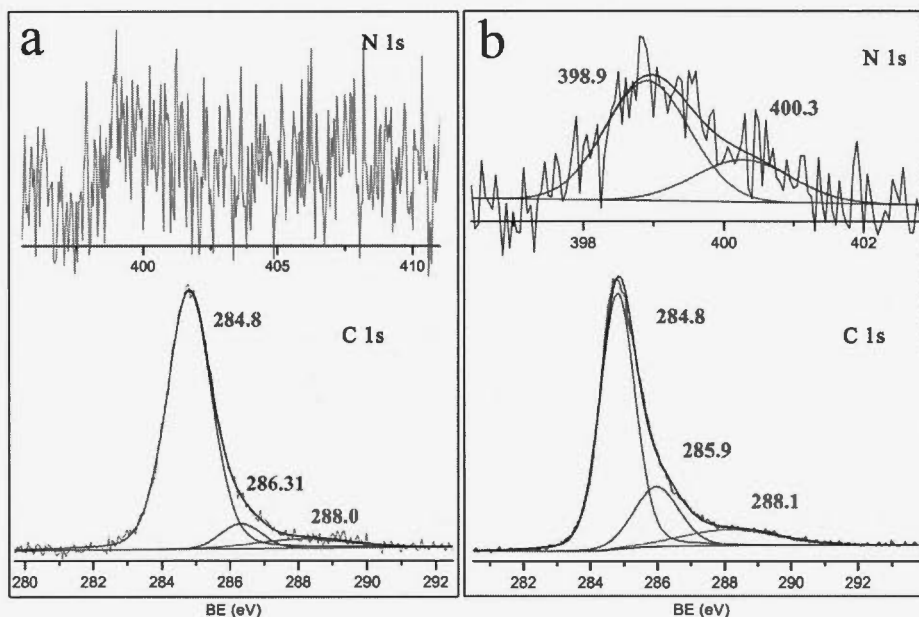


Figure 3.2: XPS characterization of N-doped graphene grown up to 30 minutes from a) pyridine, and b) dimethylformamide. The C1s peak can be split to three Lorentzian peaks labeled by red, blue, and green lines corresponding to graphite-like sp^2 C, N_{sp^2} -C bond and CO (due to absorbed oxygen) respectively. The N1s peak can be split to Lorentzian corresponding to pyridinic, pyrrolic and graphitic forms labeled by red, blue and green lines respectively.

The fraction of nitrogen contained in graphene, defined as the N/C ratio in atomic percent %, is estimated from the integrated areas of the nitrogen (N1s) and carbon (C1s) XPS peaks. The N/C ratio is found to be 5.65 %, 6.94 %, and 9.64 % for pyridine, N-methylimidazole and ethylenediamine precursors respectively. In the case of dimethylformamide, the N/C ratio is estimated to be less than 1 %. Notably, we observe that the higher the N/C ratio in the precursor, the higher the N/C ratio in the graphene, with the exception of oxygen containing dimethyl-

formamide. The D' peak in the Raman spectrum, which is related to nitrogen insertion, is found to follow the same trend as in XPS with ethylenediamine, N-methylimidazole, and pyridine showing successively less intense D' peaks. Our XPS and Raman analysis suggests that it is advantageous to use precursors with high N/C ratios to increase the nitrogen content of N-graphene. A likely advantage to N-graphene growth with precursors containing both carbon and nitrogen, as compared to gas mixtures, is the ability to control with great precision the reactant N/C ratio.

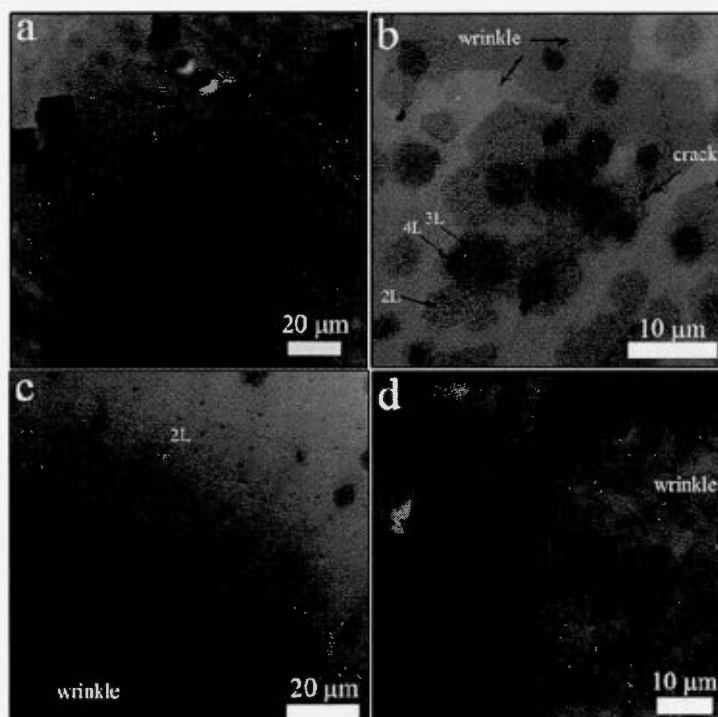


Figure 3.3: SEM image of a) the fast nucleation after 3 minutes of growth on copper, the second and third layers are seen clearly over the first layer. b) Transferred film grown from ethylenediamine after 30 min at 5 Torr of H_2 pressure, large domains of bilayer, trilayer and multilayer over monolayer within several microns cover silicon dioxide. c) At 8 Torr of H_2 a few domains of bilayer N-doped graphene are seen on transferred film on silicon dioxide. d) Monolayer of N-doped graphene transferred on silicon dioxide using 10 Torr of hydrogen in the growth.

Importantly, hydrogen has a significant role in improving the quality of the resulting films (Figure 3.3) and promoting control of the N-doped graphene multilayer growth. Increasing the growth time using ethylenediamine at a low 5 Torr pressure of hydrogen yields individual multilayer domains of sufficient size to be analyzed with a confocal Raman microscope. A distinct signature is observed in the $2D$ peak, which, with respect to a monolayer, is blue shifted by 9 cm^{-1} and 13 cm^{-1} for bi-layers and tri-layers, respectively. No significant shifting for multi-layers thicker than tri-layers was observed. The $2D$ FWHM versus layer number was found to be 33 cm^{-1} for mono-layers, 48.7 cm^{-1} for bi-layers, 55.9 cm^{-1} for tri-layers and 62.4 cm^{-1} for multi-layers. The observed $2D$ peaks are comparable to that of corresponding layers of pristine graphene.(Ni et al. 2009) While a slight blue-shift is observed for the G peak, which broadens and moves toward the D' peak in multilayers. The D' peak is red-shifted, appearing at: 1624.8 cm^{-1} , 1623.8 cm^{-1} , 1623.1 cm^{-1} and 1622.8 cm^{-1} for mono-layers through to multi-layers (the multi-layer peak being extracted by curve fitting).

3.2.2 Raman

The most prominent peaks in the Raman spectra of N-graphene (Figure 3.4) are the $2D$ appearing at 2686.3 cm^{-1} , the G at 1585.7 cm^{-1} , the D at 1348.4 cm^{-1} , and the D' at 1624.8 cm^{-1} . The FWHM of the $2D$ peak in N-graphene is broadened to 33 cm^{-1} , as compared to the 29.3 cm^{-1} FWHM for pristine graphene. The intensity ratio of the $2D$ peak to the G peak, I_{2D}/I_G , is 1.74 which is characteristic of monolayer graphene.(Graf *et al.*, 2007) This value is less than 3.43 of pristine graphene. The ratio of D peak to G peak intensity, I_D/I_G , of N-graphene is 0.20 indicating the breaking of graphene lattice symmetry by nitrogen incorporation.

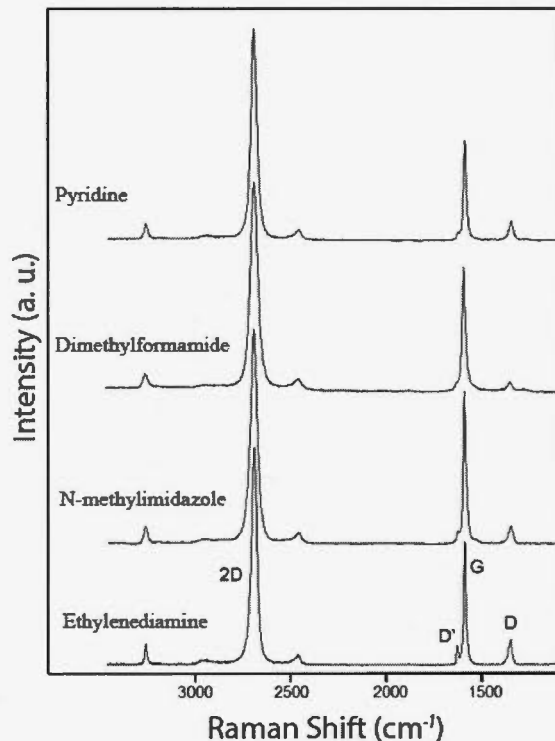


Figure 3.4: Raman spectra of monolayer N-doped graphene using precursors: pyridine, dimethylformamide, N-methylimidazole and ethylenediamine. The measurements were performed on films transferred on silicon dioxide.

3.3 Conclusion

In summary it was shown that it is possible to grow N-doped graphene using many precursors containing at least one nitrogen atom. The percentage of doping depends on carbon nitrogen ratio in each precursor. The ethylenediamine with high N/C ratio provide the best percentage of doping in this study. Under high flow of hydrogen it's possible to control the growth of only one layer and improve its quality. Furthermore, hydrogen has an important role in controlling the growth of multilayer N-doped graphene layers. Large domains of bilayers, trilayers and multilayers of N-doped graphene were shown, for which a clear Raman spectroscopy fingerprint was determined. Advanced investigations are needed to improve the

doping of graphene by nitrogen within graphitic configuration in order to tailor the semiconductor behavior of pristine graphene.

CHAPTER IV

EFFECT OF THE SIMULTANEOUS PRESENCE OF OXYGEN, CARBON, AND NITROGEN MOIETIES DURING CVD GRAPHENE GROWTH

4.1 Preliminary results

As it was shown thus far for the synthesis of graphene by CVD, the presence of oxygen, carbon, and hydrogen in the same precursor produces a material as good as the reference (methane). Furthermore, replacing oxygen with nitrogen results in high quality n-doped graphene.

During the experiments conducted for the synthesis of n-graphene, the precursor dimethylformamide was considered and tested. High-quality graphene films were obtained, confirmed by Raman spectroscopy and XPS, with no trace of n-doping, *i.e.* no appearance of the D' peak at 1625 cm^{-1} , and no N1s signal in XPS. Naturally, an investigation was conducted, parts of which are presented in this chapter.

The main directive was to choose precursors containing different ratios of C:N:O atoms. Nitromethane, an azeotropic mixture of ethylenediamine (82%) with water, nitrobenzene (BzNO_2), aniline (BzNH_2), phenol (BzOH), and benzene (Bz, as a reference) were used as precursors for the CVD synthesis of graphene. The benzene moiety was selected to show the influence of excess carbon atoms, while the rest of the precursors give information on the effect of the different ratios.

Table 4.1: Atomic ratios (C:N:O) for the different precursors used.

Precursor	CH ₃ NO ₂	EDA/H ₂ O	BzNO ₂	BzNH ₂	BzOH	Bz
Ratio C:N:O	1 : 1 : 2	3 : 3 : 1	6 : 1 : 2	6 : 1 : 0	6 : 0 : 1	6 : 0 : 0

4.2 Results and discussion

First, the graphene synthesis from DMF was reproduced. The Raman analysis of these samples indicates that the obtained graphene is of comparable quality to the methane reference. Slight to no doping is also observable. An initial conclusion is that there is a potential inhibiting effect of the oxygen on the doping process, which lead to establishing a series of experiments in order to obtain better insight. In standard graphene growth conditions, nitromethane and the EDA/H₂O azeotrope do not lead to the formation of any carbon film, as shown by the Raman spectroscopy measurements (Figure 4.10), in which the characteristic graphene peaks (1350 cm⁻¹, 1580 cm⁻¹, and 2700 cm⁻¹) are missing. Nitromethane and EDA/H₂O synthesis show the formation of craters on the surface of the copper catalyst (Figure 4.3).

After synthesis with CH₃NO₂ and EDA/H₂O the surface of the catalyst undergoes structural changes. The initial smooth finish becomes covered in holes of various sizes as seen in Figure 4.2. This indicates that some unforeseen processes take place at copper's surface in these conditions; they are either kinetically or thermodynamically favourable.

Moreover, the catalyst films change their physical conformation. What is inserted in the reaction chamber as initially flat, becomes rolled downwards from the edges perpendicular to the gas flow. This is representative of a stress endured by the copper's polycrystalline structure. Such behaviour can be observed when, for instance, a bilayer material is formed using layers of polymers with different

expansion coefficients. Upon heating the material, the layer with the largest expansion coefficient encounters resistance from the opposing layer. This causes the whole system to bend, and the surface with the fast-expanding polymer takes a concave shape.

Although the catalyst's behaviour is an interesting subject for more studies, my interest was limited to the formation of carbon species, especially graphene, on its surface. XPS analysis was performed on several samples, the focus being turned towards C1s and N1s species.

4.2.1 XPS

Nitromethane samples give a C1s signal which can be separated in 3 individual peaks (Figure 4.1). The peak at 283.8 eV can be attributed to CN species. (Mekhalif *et al.*, 2001) Secondly, the peak at 285.1 eV is typical of $C_{sp^2}-N_{sp^2}$ and $C-NH_2$ species. (Luo *et al.*, 2011) The lack of a peak at 284.6 eV can indicate the absence of $C_{sp^2}=C_{sp^2}$ bonds from graphitic carbon. Lastly, the third deconvoluted peak can be assigned to NCO moieties, as well as to CN, CO, and CO_2 which can also originate from surface adsorption. (Carley *et al.*, 2003)

Similarly, the C1s data from methane-sourced graphene shows a peak around 287.2 eV which is attributable to atmospheric CO_n ($n=1, 2$) species. Notable is also the large intensity difference between the data set for nitromethane and methane. There are more oxygen-rich species on the nitromethane-sourced samples which can interfere with the graphene-forming catalytic reaction at the copper's surface.

As far as nitrogen is concerned, the N1s data for the nitromethane-sourced samples presents a large signal around 398 eV. Its deconvolution can be interpreted

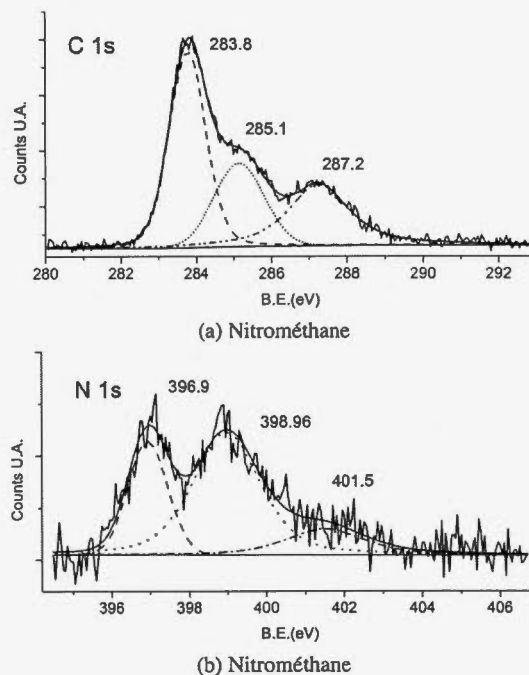


Figure 4.1: C1s and N1s XPS spectra of copper samples after CVD reaction with nitromethane.

through three components. The peak at 396.9 eV confirms the presence of CN species (Roberts, 1977) The second peak at 398.0 eV indicates the presence of C–NH₂ or C–N_{sp²} species. (Wu *et al.*, 2012) Lastly, the peak at 401.5 eV is representative of NO_x species (x = 1, 2). (Roberts, 1977) It can partly be concluded that the growth attempt with nitromethane will not be successful due to the formation of a large number of non-plane forming bonds, most likely amorphous, non-graphitizing carbon species with a large content of O and N.

The EDA/H₂O mixture has an analogous behaviour presenting similar deconvolutions for both its N1s and C1s XPS high resolution spectra. The carbon band can be deconvoluted in three peaks at 284.4 eV, 285.5 eV, and 287.4 eV, which can possibly be attributed to graphitizing C–C bonds, C–N_{sp²} bonds, and CO, CO₂ species respectively. Its N1s band around 400 eV can be deconvoluted in three

peaks as well. The first at 398.3 eV can be attributed to pyridinic N in a graphitic structure.(Luo *et al.*, 2011, Jin *et al.*, 2011) The following peak at 400.3 eV indicates the presence of pyrrolic N,(Luo *et al.*, 2011) and the last peak at 402.1 eV indicates graphitic N.(Roberts, 1977) This analysis indicates the presence of various CN species, mostly graphitic.

4.2.2 SEM imagery

The copper samples after nitromethane reactions presented a unique surface morphology responsible for the samples' curvature. Simple optical imagery did not provide clear enough information due to a lack of polarization, thus Scanning Electron Microscopy was used.

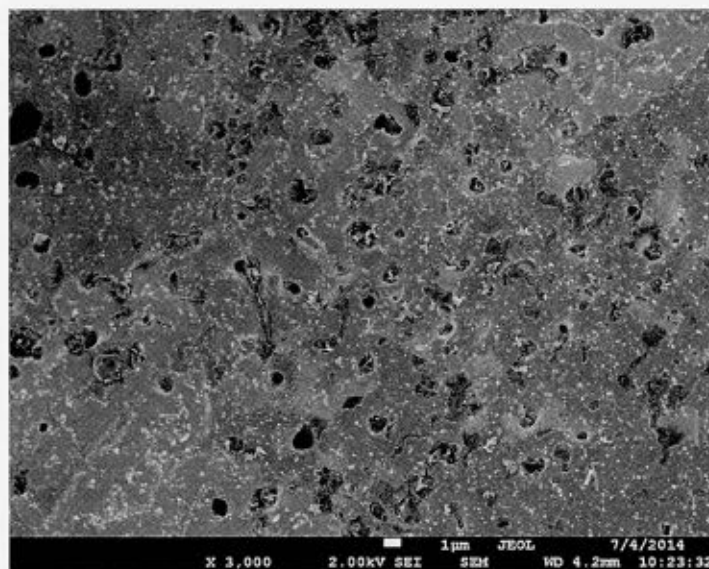


Figure 4.2: SEM image of a copper sample after having been exposed to a 15 minute CVD reaction with nitromethane.

A 15 minute reaction shows a rough surface, presenting copper deformations, holes, and various surface structures (Figure 4.2).

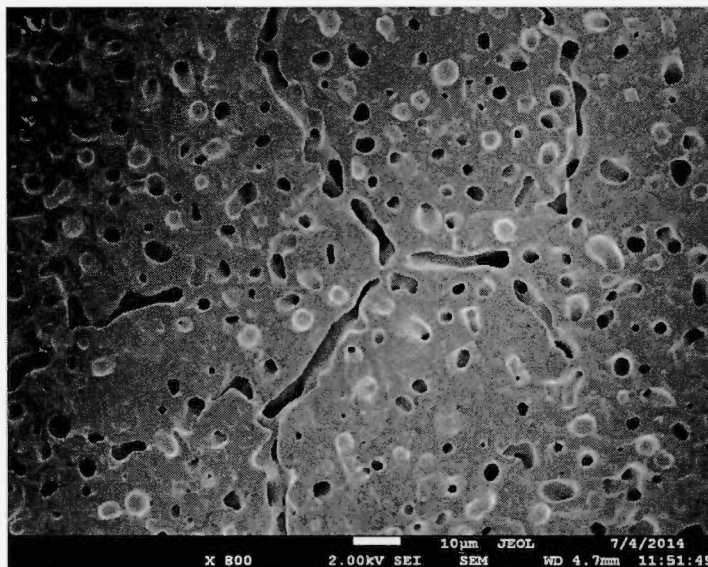


Figure 4.3: SEM image of a copper sample after having been exposed to a 30 minute CVD reaction with nitromethane.

From 30 minutes of reaction time, the copper surface starts to become smoother. The formed holes are more pronounced, they seem to start eroding the surface from the copper's crystalline grain boundaries. Moreover, a hint of activity beneath the surface is seen, giving the sheet a sponge-like structure at its surface (Figure 4.3).

The surface morphology of copper starts to remain consistent from 30 minutes reaction and more. This can be seen in Figure 4.4 presenting the surface after a 45 minute reaction. The same behaviour as before is observed, with holes at different stages of formation following the grain boundaries and continuing beneath the smooth surface.

From 60 minutes on (Figure 4.5) the surface smoothness starts to influence the holes' overall aspect. Some holes start to close, and the eroded edges lose homogeneity. This is an indicator of metal migration at the surface due to the high energy in the system. Moreover, it is evident that the kinetics of the corrosion are fast enough to leave a mark on the surface before the metal migration covers

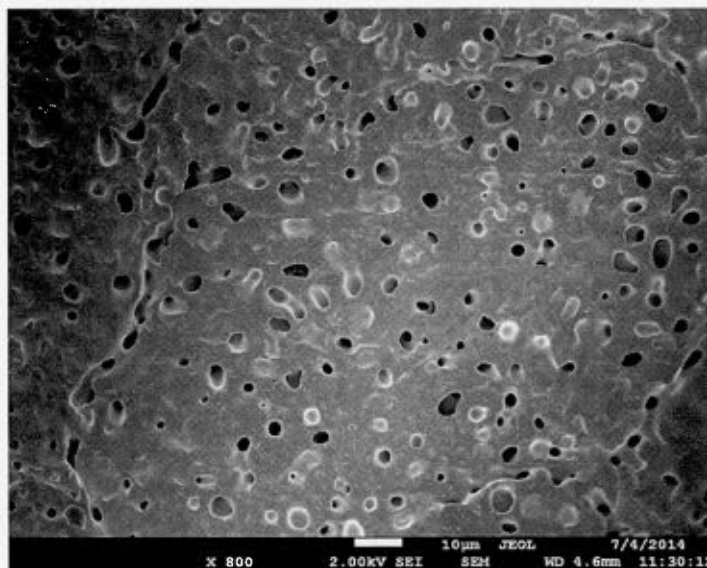


Figure 4.4: SEM image of a copper sample after having been exposed to a 45 minute CVD reaction with nitromethane.

them. This behaviour is better seen in Figure 4.6 showing the copper surface after 75 minutes of growth. Its smooth surface and smaller holes indicate matter migration, most likely due to melting of the copper's surface.

Statistical measurements of the holes' sizes were made over 63 randomly picked holes for each growth period; for 15 minutes only 10 holes were measured due to a lack of population. The results are illustrated in Figure 4.7.

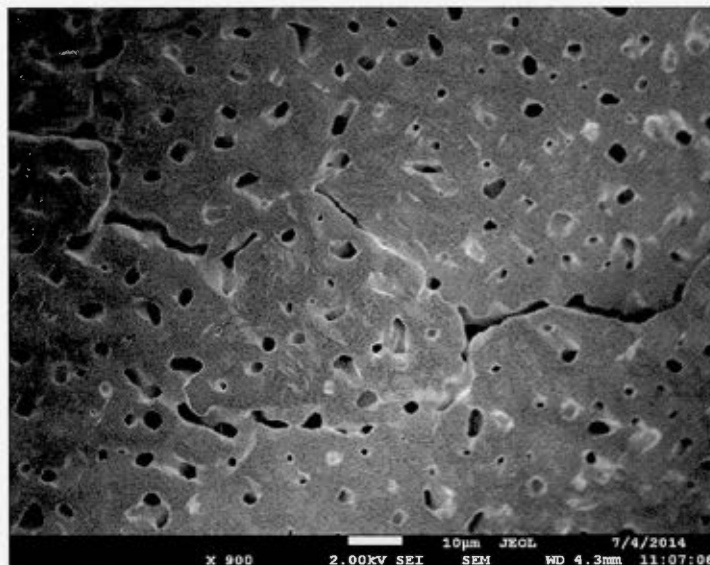


Figure 4.5: SEM image of a copper sample after having been exposed to a 60 minute CVD reaction with nitromethane.

The size of the pores increases up to a reaction time of 30 minutes as seen in Figure 4.7. A longer reaction time leads to the shrinkage of the pore size. From this it can be postulated that the corrosion is most important during the first 30 minutes after which it reaches a limit. The dominating surface process then most likely remains the surface diffusion of the metal. It is, however, naïve to suggest that chemical processes stop after a certain time. Considering the Raman and XPS data, it is obvious that no graphene is formed. As of yet, a clear presentation of the surface phenomena leading to the corrosion has not been made, however, a connection to oxygen's presence can be postulated.

For several growth periods 8 samples per duration were weighed to study the mass loss after the reaction (Figure 4.8). The samples were weighed before and after reaction (4 significant digits measurements), then the ratio of loss was calculated following the equation $(m_{initial} - m_{final})/m_{initial}$. The scatter plots of mass loss ratio versus time followed an exponential fit (not shown), thus a logarithmic plot of \ln of the mass loss ratio versus time seemed more appropriate.

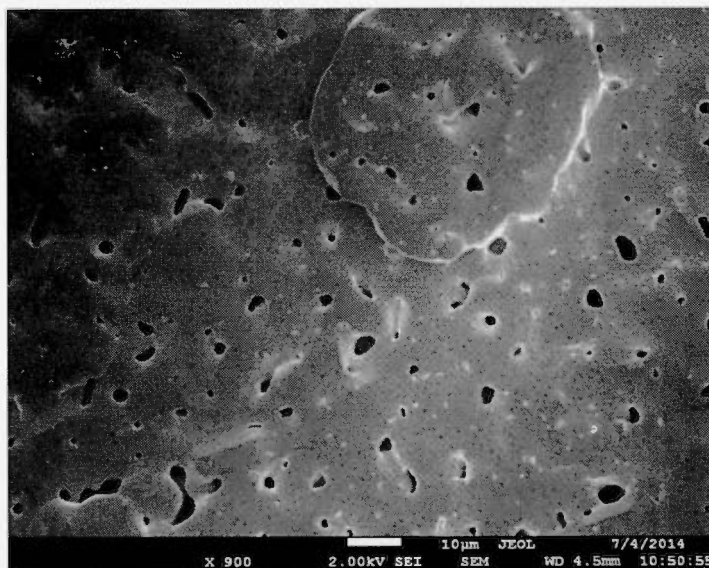


Figure 4.6: SEM image of a copper sample after having been exposed to a 75 minute CVD reaction with nitromethane.

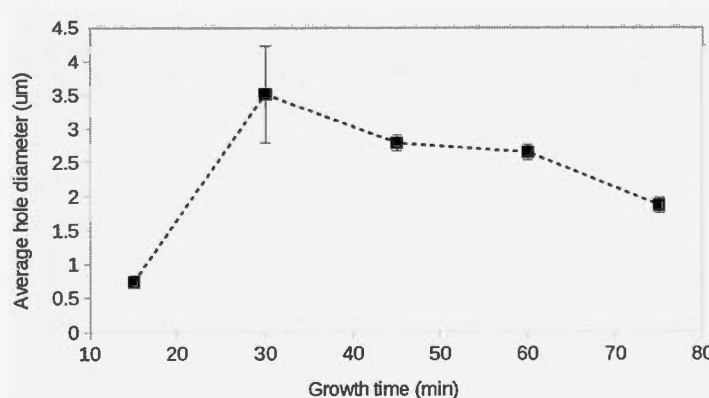


Figure 4.7: Average hole diameter versus CVD growth time on copper samples using nitromethane as a precursor. Sample sizes of 10 (for 15 minutes) and 63 holes (30, 45, 60, 75 minutes).

The logarithmic linearity in Figure 4.8 indicates a first-order reaction behaviour. In the case of nitromethane a plateau is reached after 60 minutes of reaction time. Its mass loss rate is considerably larger than in the case of the methane-sourced reactions. To note as well, the mean errors evolution seems proportional to the increased reaction time.

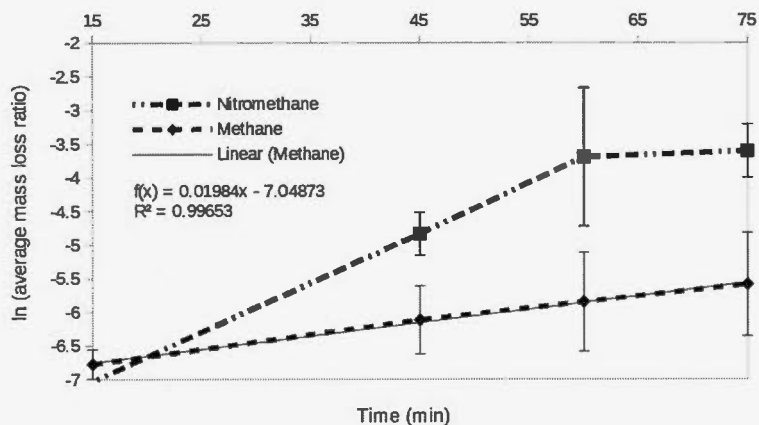


Figure 4.8: Mass loss statistics of 8 samples per reaction duration (15, 45, 60, 75 minutes), for nitromethane and methane sourced CVD reactions. For visualization convenience, mean error bars were multiplied by a factor of 1000 for CH_4 , 100 for CH_3NO_2 and the last data point at 75 °C by a factor of 10.

4.2.3 Raman

Raman spectra were taken at a 514 nm wavelength.

Spectra were taken after a 15 minute growth with nitromethane. A high intensity of the *D* peak and the three peaks around 3000 cm^{-1} (Figure 4.9) indicate that the carbon species present is graphitic in nature. The spectra resemble those of typical few-layer graphene oxide. This means that the carbon species' crystal structure is highly defective, the majority of the defects arising from the material's oxidation. These can be assigned to the heterogeneous structures on the surface of the copper observed in Figure 4.2.

Increasing the reaction time leads to the disappearance of the graphitic material, probably due to its oxidation into CO , CO_2 and other volatile moieties.

In order to study the effect of an excess of carbon atoms, reactions were conducted with benzene, phenol, aniline, and nitrobenzene in similar conditions. Their Ra-

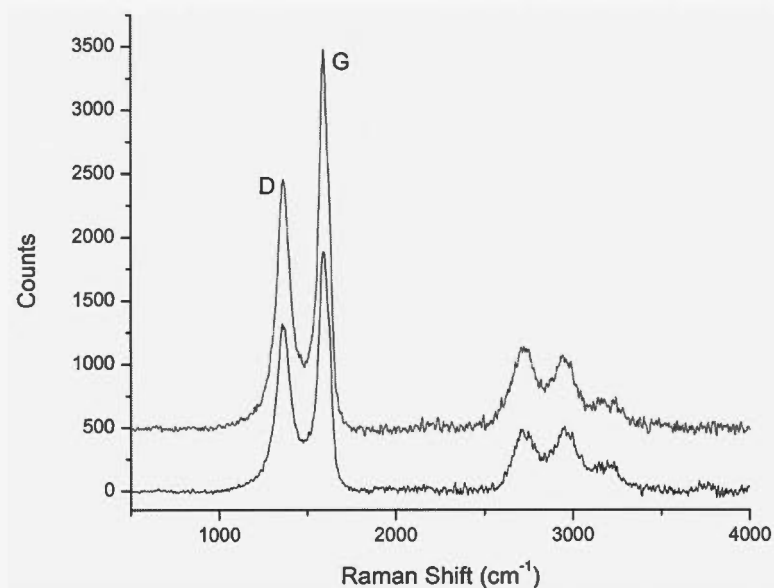


Figure 4.9: Two Raman spectra after a 15 minutes nitromethane-sourced CVD reaction on copper samples.

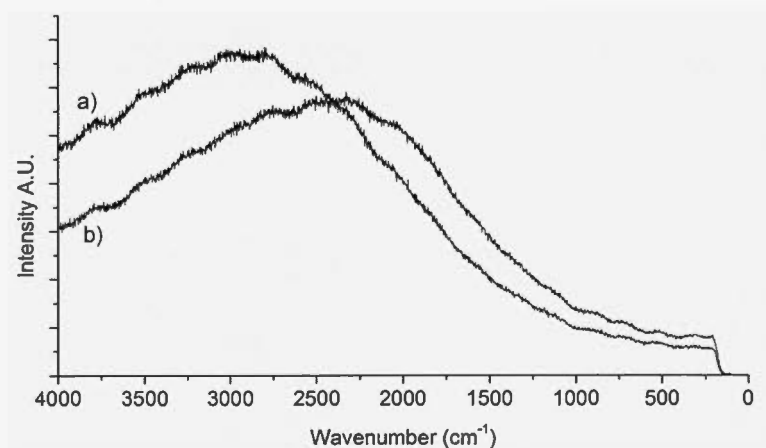


Figure 4.10: Raw Raman spectral data on copper samples having passed through a CVD growth using a) nitromethane and b) EDA/H₂O mixture for a duration of 2 hours. Only the copper's Raman background is visible.

man signatures are shown in Figure 4.11. A significant similarity is observed in all samples. Note the slight *2D* red-shift for aniline and phenol, and the presence of a shoulder around 1626 cm⁻¹ for all but methane. The XPS studies of these samples illustrate a wide variety of oxidised graphitic carbon, and oxidised nitro-

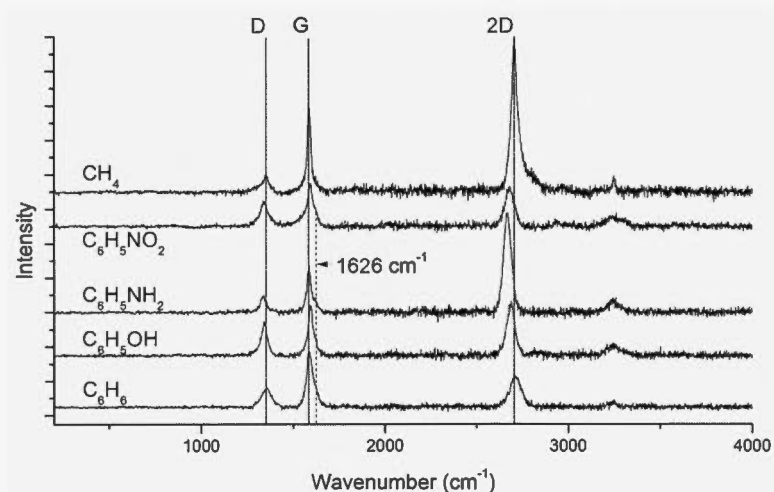


Figure 4.11: Raman spectra on copper samples after standard CVD reactions with methane, benzene, phenol, aniline, and nitrobenzene; performed under similar conditions as the methane growth.

gen species, spectra shown in the Appendices section. These species can create the shoulder at 1626 cm^{-1} as the graphitic crystal symmetry breaks due to the presence of the hetero-atoms.

4.3 Conclusion

Copper sheets were exposed to several precursors in conditions harsh enough for them to crack and undergo a catalytic reaction on the surface. Nitromethane and ethylenediamine/water azeotrope, with C:N:O ratios of 1:1:2 and 3:3:1 respectively, do not produce pristine graphene, or other carbonaceous species for that matter, following a 2 hours CVD reaction. It appears that a graphitic film is initially formed, within 15 minutes, which is then subsequently oxidised – this was observed with nitromethane. This time frame is not long enough to allow the formation of pristine graphene; however, the XPS analysis shows the presence of carbon species on the sample. The nature of these species could not be determined with certainty. A more exhaustive study is desirable in order to understand the behaviour of the surface atoms on the copper sheets.

CONCLUSION

Graphene synthesis by CVD has been extensively studied over the last decade. A point has been reached where the precursors become continuously complex stemming from the need to develop new materials and techniques.

First, graphene's synthesis has been proven possible using precursors which contain oxygen, such as aliphatic alcohols. Given the reactive nature of oxygen, one would not believe their use as fruitful. Nevertheless, pristine graphene has been obtained in certain conditions. Moreover, the procedure is faster and safer than using methane or acetylene. Obviously, the environmental pressure and vector gas play a role in the success of alcohol graphene growth. Hydrogen is generally present in excess, and in this situation capable of carrying some part of the burden which is keeping oxygen away from the catalytic process. Given the highly energetic state of the molecules in the CVD reaction chamber, it is significantly difficult to determine with acceptable certainty the process which allows for such an insignificant effect of oxygen.

Secondly, nitrogen, the most abundant atom in our atmosphere, is capable of giving graphene production a highly desirable trait, that of doping. Doped graphene is more suitable for electronic applications due to the electronic contribution of nitrogen. The production of such a material has been achieved with various precursors containing carbon and nitrogen together in various ratios: ethylenediamine, methylamine, imidazole, pyridine, etc. This behaviour is easier to comprehend af-

ter a short glance on the periodic table - both elements are neighbours, their electronic configuration differs by one electron. This allows nitrogen to effortlessly insert itself in the crystal structure of graphene. The demise of this process, though, is the chaotic, random aspect of how atoms are mixed on the catalyst's surface. There isn't any well-defined or controllable doping pattern, and the doping percentages vary considerably with system, precursor, and conditions.

Finally, the combination of all three seems to produce a different effect. In early time frames of the CVD reaction there is the general tendency to produce graphitic films. These, however, are consumed if no excess carbon is around to protect them by reacting with the oxygen, for instance; it was shown when using benzene, aniline, nitrobenzene, and phenol as precursors. Adding to this, the most important element in this reaction remains to be studied - copper - the one undergoing chemical as well as morphological changes at its surface.

In the end, this research showed that the graphene growing catalytic process taking place on copper's surface presents levels of intricacy which require a more extensive selection of experiments in order to understand, a challenge for future projects.

APPENDICE A

XPS SPECTRA OF VARIOUS SAMPLES HAVING PASSED THROUGH A CVD REACTION

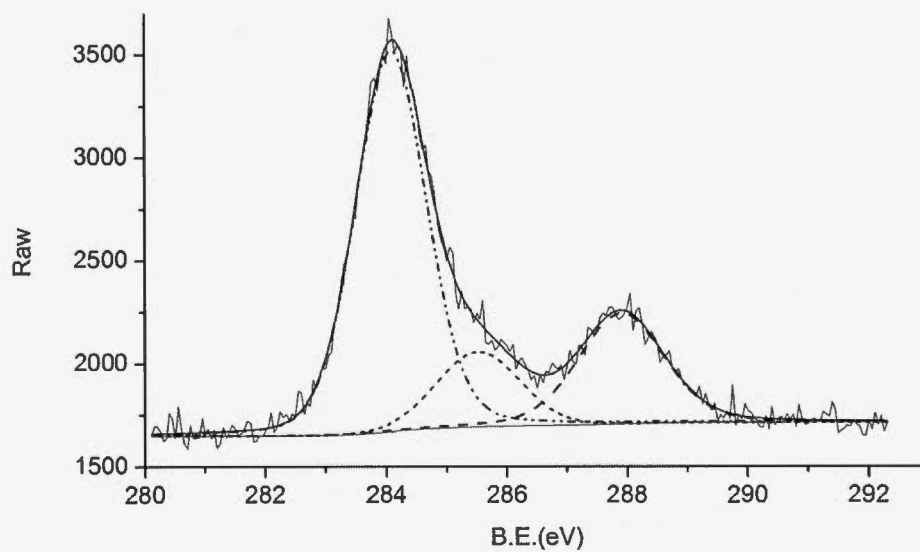


Figure A.1: C1s XPS of benzene-sourced CVD sample.

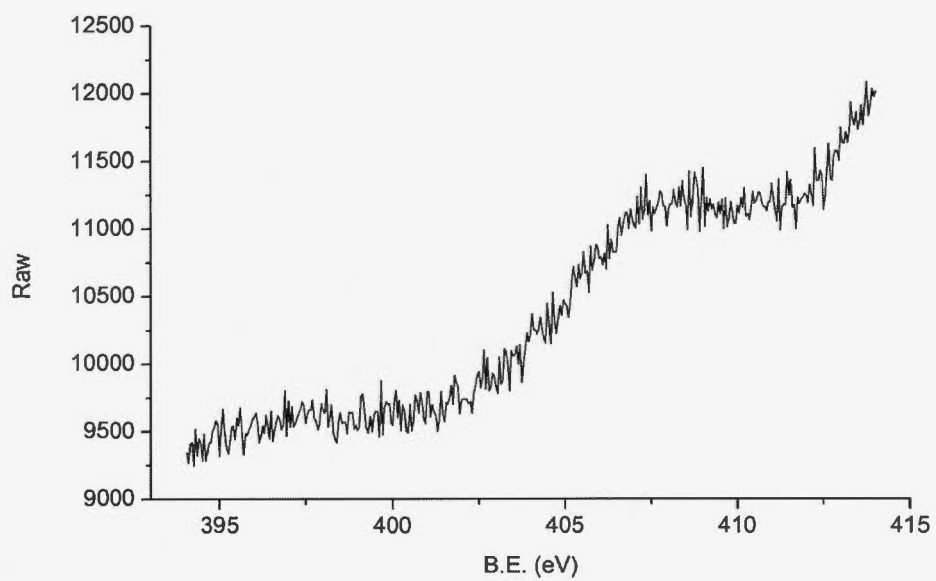


Figure A.2: N1s XPS of benzene-sourced CVD sample.

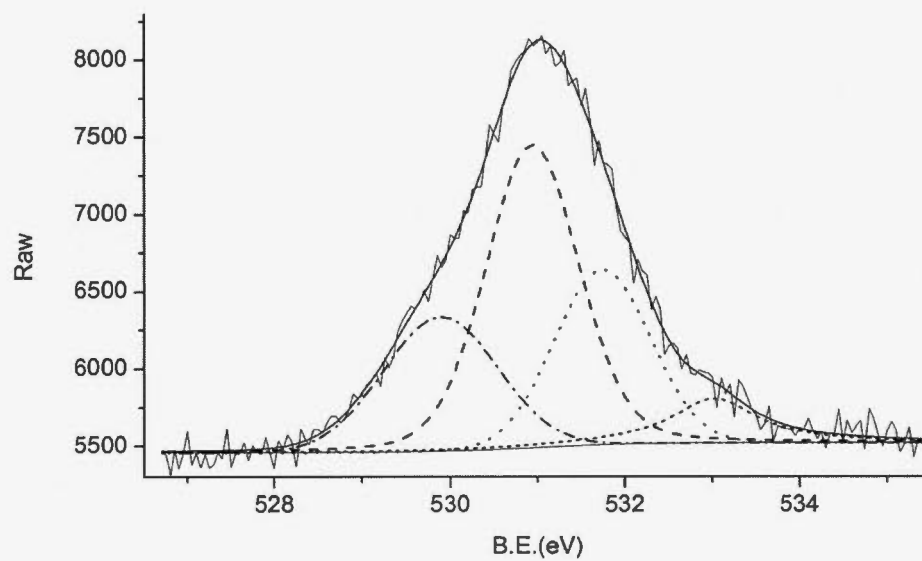


Figure A.3: O1s XPS of benzene-sourced CVD sample.

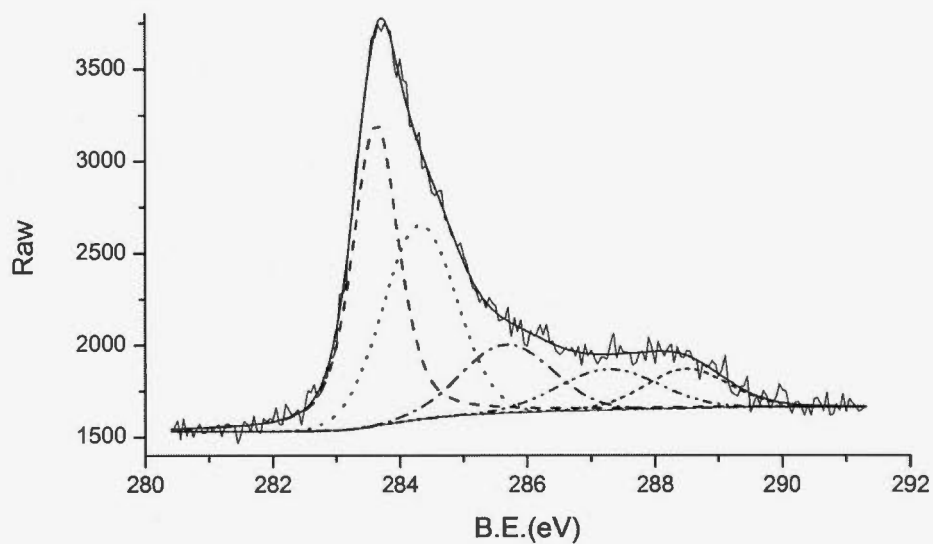


Figure A.4: C1s XPS of aniline-sourced CVD sample.

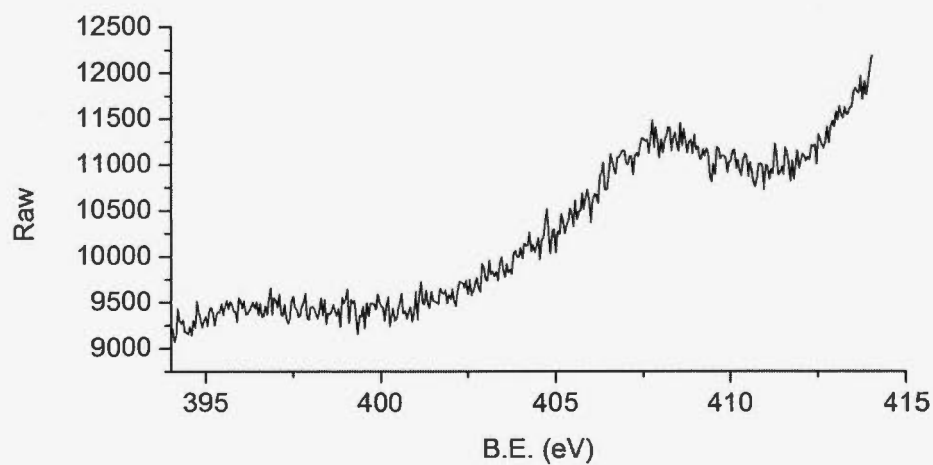


Figure A.5: N1s XPS of aniline-sourced CVD sample.

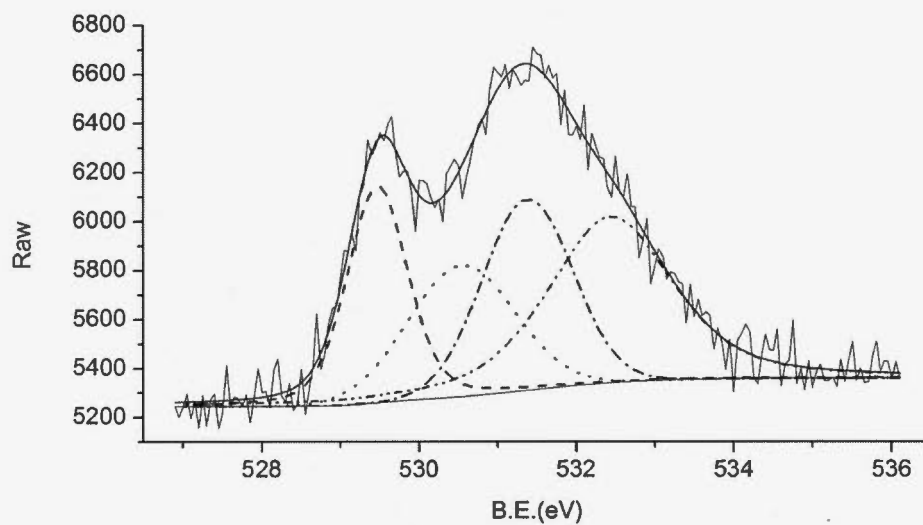


Figure A.6: O1s XPS of aniline-sourced CVD sample.

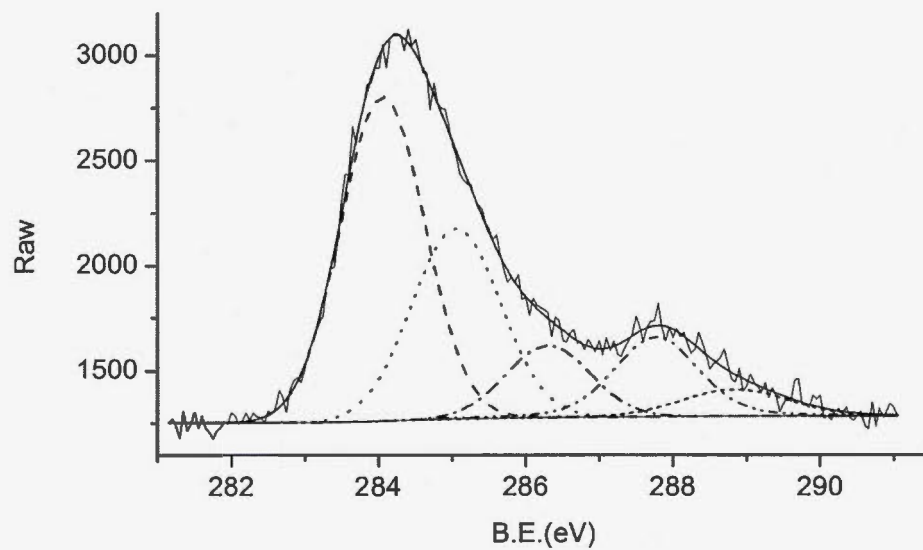


Figure A.7: C1s XPS of nitrobenzene-sourced CVD sample.

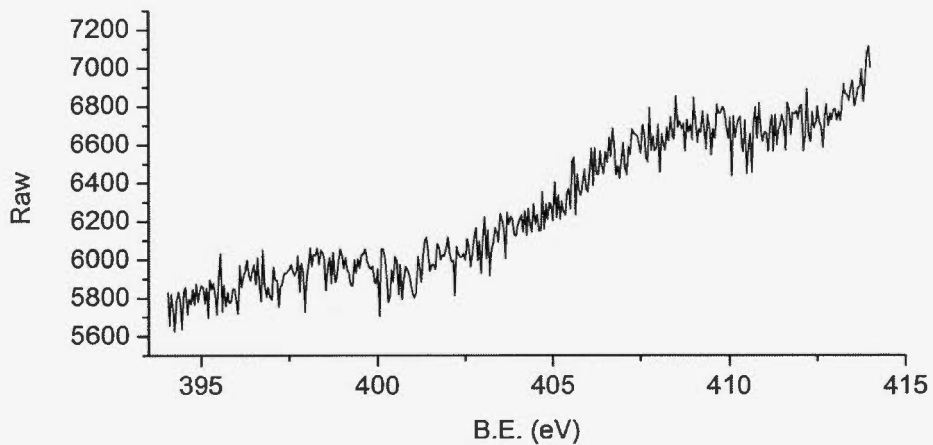


Figure A.8: N1s XPS of nitrobenzene-sourced CVD sample.

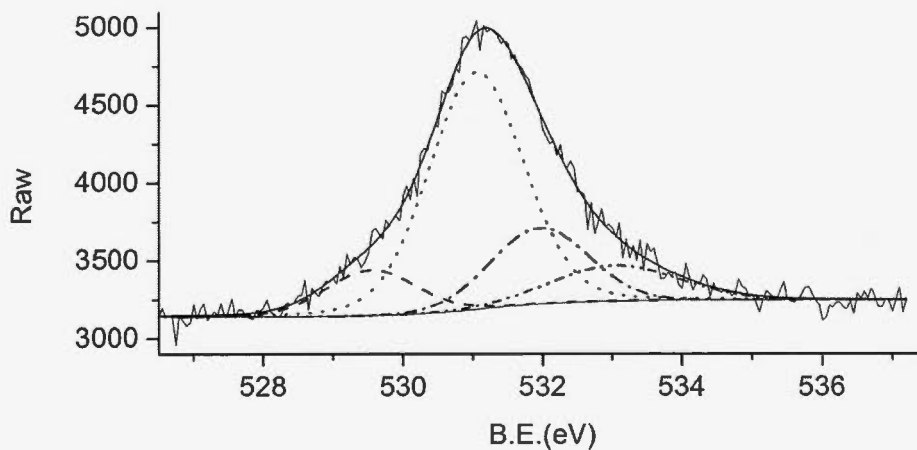


Figure A.9: O1s XPS of nitrobenzene-sourced CVD sample.

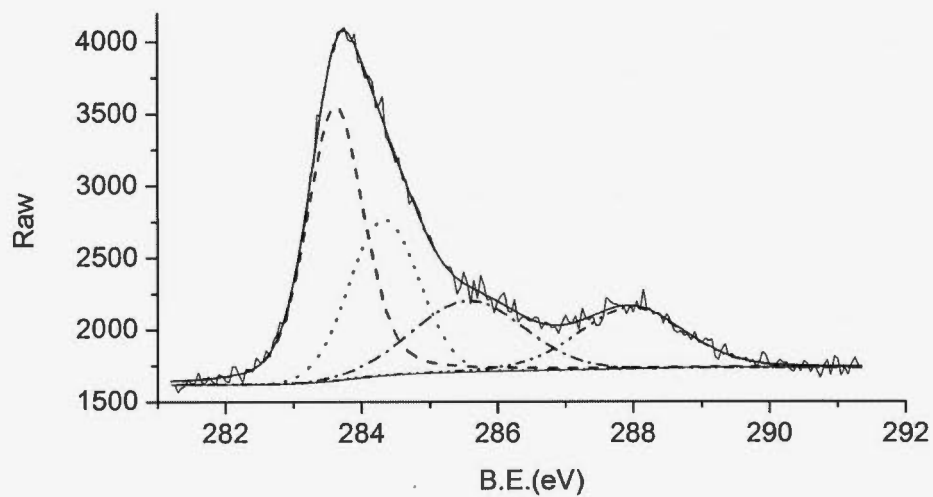


Figure A.10: C1s XPS of phenol-sourced CVD sample.

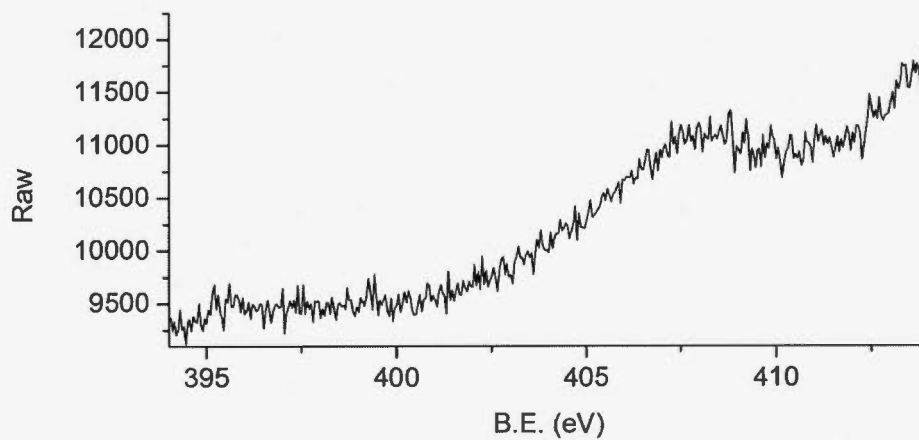


Figure A.11: N1s XPS of phenol-sourced CVD sample.

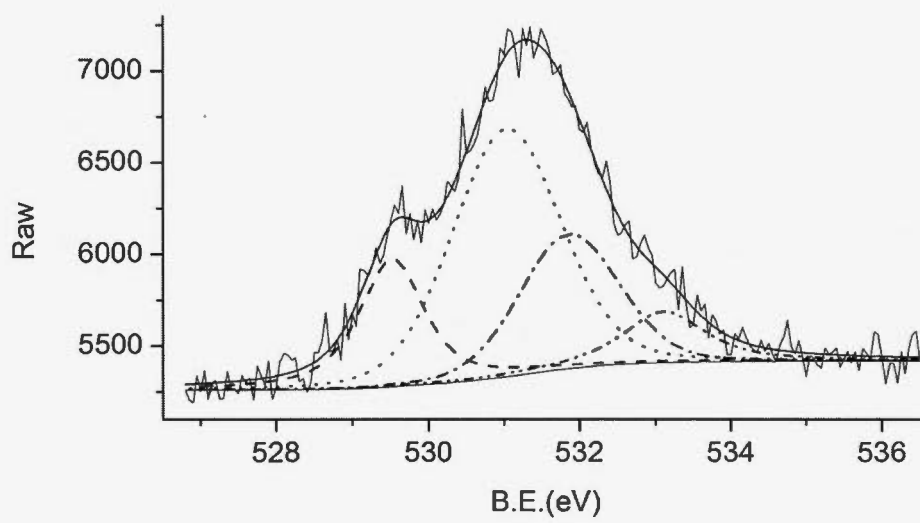


Figure A.12: O1s XPS of phenol-sourced CVD sample.

BIBLIOGRAPHY

- Avouris, P. Dimitrakopoulos, C. (2012). Graphene: synthesis and applications. *Materials Today*, 15(3), 86–97. [http://dx.doi.org/10.1016/S1369-7021\(12\)70044-5](http://dx.doi.org/10.1016/S1369-7021(12)70044-5). Available from:<http://linkinghub.elsevier.com/retrieve/pii/S1369702112700445>
- Bautista, C. Mendoza, D. (2011). Multilayer Graphene Synthesized by CVD Using Liquid Hexane as the Carbon Precursor. 2011(November), 6. <http://dx.doi.org/10.4236/wjcmp.2011.14023>. Available from:<http://arxiv.org/abs/1109.1318>
- Binnig, G. Quate, C. F. (1986). Atomic Force Microscope. *Physical Review Letters*, 56(9), 930–933. <http://dx.doi.org/10.1103/PhysRevLett.56.930>
- Bratt, A. Barron, A. R. (2011). XPS of Carbon Nanomaterials. *OpenStax CNX*. Available from:<http://cnx.org/contents/fdddbf98-39ce-4edc-934e-dd1f7477b52b02>
- Byun, S.-j., Lim, H., Shin, G.-y., Han, T.-h., Oh, S. H. Ahn, J.-h. (2011). Supporting Information Graphenes Converted from Polymers. 1–11.
- Carley, A. F., Chinn, M. Parkinson, C. (2003). The adsorption and oxidation of cyanogen on copper surfaces. *Surface Science*, 537(1-3), 64–74. [http://dx.doi.org/10.1016/S0039-6028\(03\)00533-8](http://dx.doi.org/10.1016/S0039-6028(03)00533-8). Available from:<http://linkinghub.elsevier.com/retrieve/pii/S0039602803005338><http://www.sciencedirect.com/science/article/pii/S0039602803005338>
- Chesnokov, S. A., Nalimova, V. A., Rinzler, A. G., Smalley, R. E. Fischer, J. E. (1999). Mechanical Energy Storage in Carbon Nanotube Springs. *Physical Review Letters*, 82(2), 343–346. Available from:<http://link.aps.org/doi/10.1103/PhysRevLett.82.343>
- Chung, D. D. L. (2002). Review: Graphite. <http://dx.doi.org/10.1023/A:1014915307738>
- Cooper, D. R., D'Anjou, B., Ghattamaneni, N., Harack, B., Hilke, M., Horth, A., Majlis, N., Massicotte, M., Vandsburger, L., Whiteway, E. Yu, V. (2012).

- Experimental Review of Graphene. *ISRN Condensed Matter Physics*, 2012, 1–56. <http://dx.doi.org/10.5402/2012/501686>. Available from:<http://www.hindawi.com/journals/isrn.cmp/2012/501686/>
- Cui, T., Lv, R., Huang, Z.-H., Zhu, H., Kang, F., Wang, K.Wu, D. (2012). Effect of feed rate on the production of nitrogen-doped graphene from liquid acetonitrile. *Carbon*, 50(10), 3659–3665. <http://dx.doi.org/10.1016/j.carbon.2012.03.038>. Available from:<http://linkinghub.elsevier.com/retrieve/pii/S0008622312002862>
- Dong, X., Fu, D., Fang, W., Shi, Y., Chen, P.Li, L.-J. (2009). Doping Single-Layer Graphene with Aromatic Molecules. *Small*, 5(12), 1422–1426. <http://dx.doi.org/10.1002/sml1.200801711>. Available from:<http://dx.doi.org/10.1002/sml1.200801711>
- Dong, X., Wang, P., Fang, W., Su, C.-Y. Y., Chen, Y.-H. H., Li, L.-J. J., Huang, W.Chen, P. (2011). Growth of large-sized graphene thin-films by liquid precursor-based chemical vapor deposition under atmospheric pressure. *Carbon*, 49(11), 3672–3678. <http://dx.doi.org/10.1016/j.carbon.2011.04.069>. Available from:<http://linkinghub.elsevier.com/retrieve/pii/S0008622311003460><http://dx.doi.org/10.1016/j.carbon.2011.04.069>
- Egerton, R. F. (2005). *Physical principles of electron microscopy*. Springer. <http://dx.doi.org/10.1007/b136495>. Available from:[http://scholar.google.com/scholar?hl=en&btnG=Search&q=intitle:No+Title\#0\\$\backslash\\$http://link.springer.com/content/pdf/10.1007/b136495.pdf](http://scholar.google.com/scholar?hl=en&btnG=Search&q=intitle:No+Title\#0\backslashhttp://link.springer.com/content/pdf/10.1007/b136495.pdf)
- Falcao, E. H. L. Wudl, F. (2007). Carbon allotropes: beyond graphite and diamond. *Journal of Chemical Technology & Biotechnology*, 82(6), 524–531. <http://dx.doi.org/10.1002/jctb.1693>. Available from:<http://dx.doi.org/10.1002/jctb.1693>
- Ferrari, A. C. (2007). Raman spectroscopy of graphene and graphite: Disorder, electron–phonon coupling, doping and nonadiabatic effects. *Solid State Communications*, 143(1-2), 47–57. <http://dx.doi.org/10.1016/j.ssc.2007.03.052>. Available from:<http://linkinghub.elsevier.com/retrieve/pii/S0038109807002967>
- Ferrari, A. C., Meyer, J. C., Scardaci, V., Casiraghi, C., Lazzeri, M., Mauri, F., Piscanec, S., Jiang, D., Novoselov, K. S., Roth, S.Geim, a. K. (2006). Raman Spectrum of Graphene and Graphene Layers. *Physical Review Letters*, 97(18), 187401. <http://dx.doi.org/10.1103/PhysRevLett.97.187401>. Available from:<http://link.aps.org/doi/10.1103/PhysRevLett.97.187401>

- Gao, H., Song, L., Guo, W., Huang, L., Yang, D., Wang, F., Zuo, Y., Fan, X., Liu, Z., Gao, W., Vajtai, R., Hackenberg, K.Ajayan, P. M. (2012). A simple method to synthesize continuous large area nitrogen-doped graphene. *Carbon*, 50(12), 4476–4482. <http://dx.doi.org/10.1016/j.carbon.2012.05.026>. Available from:<http://linkinghub.elsevier.com/retrieve/pii/S0008622312004551>
- Graf, D., Molitor, F., Ensslin, K., Stampfer, C., Jungen, A., Hierold, C.Wirtz, L. (2007). Spatially Resolved Raman Spectroscopy of Single- and Few-Layer Graphene. *Nano Letters*, 7(2), 238–242. <http://dx.doi.org/10.1021/nl061702a>. Available from:<http://dx.doi.org/10.1021/nl061702a>
- Gray, D., McCaughan, A.Mookerji, B. (2009). Crystal Structure of Graphite, Graphene and Silicon. *Physics for Solid State Applications*, 6.730.
- Guermoune, A., Chari, T., Popescu, F., Sabri, S. S., Guillemette, J., Skulason, H. S., Szkopek, T.Siaj, M. (2011). Chemical vapor deposition synthesis of graphene on copper with methanol, ethanol, and propanol precursors. *Carbon*, 49(13), 4204–4210. <http://dx.doi.org/10.1016/j.carbon.2011.05.054>. Available from:<http://linkinghub.elsevier.com/retrieve/pii/S0008622311004301>
- Han, G. H., Güneş, F., Bae, J. J., Kim, E. S., Chae, S. J., Shin, H.-J., Choi, J.-Y., Pribat, D.Lee, Y. H. (2011). Influence of copper morphology in forming nucleation seeds for graphene growth. *Nano letters*, 11(10), 4144–8. <http://dx.doi.org/10.1021/nl201980p>. Available from:<http://www.ncbi.nlm.nih.gov/pubmed/21863812>
- Imamura, G. Saiki, K. (2011). Synthesis of nitrogen-doped graphene on Pt(111) by chemical vapor deposition. *Journal of Physical Chemistry C*, 115(20), 10000–10005. <http://dx.doi.org/10.1021/jp202128f>. Available from:<http://pubs.acs.org/doi/abs/10.1021/jp202128f>
- Ismach, A., Druzgalski, C., Penwell, S., Schwartzberg, A., Zheng, M., Javey, A., Bokor, J.Zhang, Y. (2010). Direct chemical vapor deposition of graphene on dielectric surfaces. *Nano Letters*, 10(5), 1542–1548. <http://dx.doi.org/10.1021/nl9037714>. Available from:<http://www.ncbi.nlm.nih.gov/pubmed/20361753>
- Jin, Z., Yao, J., Kittrell, C.Tour, J. M. (2011). Large-scale growth and characterizations of nitrogen-doped monolayer graphene sheets. *ACS Nano*, 5, 4112–4117. <http://dx.doi.org/10.1021/nn200766e>
- John, R., Ashokreddy, a., Vijayan, C.Pradeep, T. (2011). Single- and few-layer graphene growth on stainless steel substrates by direct thermal chemical vapor

- deposition. *Nanotechnology*, 22(16), 165701. <http://dx.doi.org/10.1088/0957-4484/22/16/165701>. Available from:<http://www.ncbi.nlm.nih.gov/pubmed/21393813>
- Kang, J., Shin, D., Bae, S.Hong, B. H. (2012). Graphene transfer: key for applications. *Nanoscale*, 4(18), 5527. <http://dx.doi.org/10.1039/c2nr31317k>. Available from:<http://www.ncbi.nlm.nih.gov/pubmed/22864991>
- Kumar, A. Lee, C. H. (2013). Synthesis and Biomedical Applications of Graphene : Present and Future Trends. *Advances in Graphene Science*, 55–75. <http://dx.doi.org/10.5772/55728>
- Kwon, S. Y., Ciobanu, C. V., Petrova, V., Shenoy, V. B., Bareño, J., Gambin, V., Petrov, I.Kodambaka, S. (2009). Growth of semiconducting graphene on palladium. *Nano Letters*, 9(12), 3985–3990. <http://dx.doi.org/10.1021/nl902140j>
- Lee, D. S., Riedl, C., Krauss, B., von Klitzing, K., Starke, U.Smet, J. H. (2008). Raman spectra of epitaxial graphene on SiC and of epitaxial graphene transferred to SiO₂. *Nano letters*, 8(12), 4320–5. <http://dx.doi.org/10.1021/nl802156w>. Available from:<http://www.ncbi.nlm.nih.gov/pubmed/19368003>
- Lee, S., Lee, K.Zhong, Z. (2010). Wafer scale homogeneous bilayer graphene films by chemical vapor deposition. *Nano letters*, 10(11), 4702–7. <http://dx.doi.org/10.1021/nl1029978>. Available from:<http://www.ncbi.nlm.nih.gov/pubmed/20932046>
- Lherbier, A., Blase, X., Niquet, Y.-M. M., Triozon, F.Roche, S. (2008). Charge Transport in Chemically Doped 2D Graphene. *Physical Review Letters*, 101(3), 036808. <http://dx.doi.org/10.1103/PhysRevLett.101.036808>. Available from:<http://link.aps.org/doi/10.1103/PhysRevLett.101.036808>
- Li, R., Wei, Z., Gou, X.Xu, W. (2013). Phosphorus-doped graphene nanosheets as efficient metal-free oxygen reduction electrocatalysts. *RSC Advances*, 3(25), 9978. <http://dx.doi.org/10.1039/c3ra41079j>. Available from:<http://xlink.rsc.org/?DOI=c3ra41079j>
- Li, X., Cai, W., An, J., Kim, S., Nah, J., Yang, D., Piner, R., Velamakanni, A., Jung, I., Tutuc, E., Banerjee, S. K., Colombo, L.Ruoff, R. S. (2009a). Large-area synthesis of high-quality and uniform graphene films on copper foils. *Science (New York, N.Y.)*, 324(5932), 1312–1314. <http://dx.doi.org/10.1126/science.1171245>. Available from:<http://www.ncbi.nlm.nih.gov/pubmed/19423775>

- Li, X., Cai, W., Colombo, L., Ruoff, R. S. (2009b). Evolution of graphene growth on Cu and Ni studied by carbon isotope labeling. *Nano Letters*, 9(12), 15. <http://dx.doi.org/10.1021/nl902515k>. Available from: <http://www.ncbi.nlm.nih.gov/pubmed/19711970> <http://arxiv.org/abs/0907.1859>
- Li, Z., Wu, P., Wang, C., Fan, X., Zhang, W., Zhai, X., Zeng, C., Li, Z., Yang, J., Hou, J. (2011). Low-Temperature Growth of Graphene by Chemical Vapor Deposition Using Solid and Liquid Carbon Sources. *ACS Nano*, 5(4), 3385–3390. <http://dx.doi.org/10.1021/nn200854p>. Available from: <http://dx.doi.org/10.1021/nn200854p>
- Lin, Y.-C., Lin, C.-Y., Chiu, P.-W. (2010). Controllable graphene N-doping with ammonia plasma. *Applied Physics Letters*, 96(13), 133110. <http://dx.doi.org/10.1063/1.3368697>. Available from: <http://link.aip.org/link/APPLAB/v96/i13/p133110/s1&Agg=doi>
- Luo, Z., Lim, S., Tian, Z., Shang, J., Lai, L., MacDonald, B., Fu, C., Shen, Z., Yu, T., Lin, J. (2011). Pyridinic N doped graphene: synthesis, electronic structure, and electrocatalytic property. *Journal of Materials Chemistry*, 21(22), 8038. <http://dx.doi.org/10.1039/c1jm10845j>. Available from: <http://xlink.rsc.org/?DOI=c1jm10845j>
- Malard, L., Pimenta, M., Dresselhaus, G., Dresselhaus, M. (2009). Raman spectroscopy in graphene. *Physics Reports*, 473(5-6), 51–87. <http://dx.doi.org/10.1016/j.physrep.2009.02.003>. Available from: <http://linkinghub.elsevier.com/retrieve/pii/S0370157309000520>
- Martins, L. G. P., Song, Y., Zeng, T., Dresselhaus, M. S., Kong, J., Araujo, P. T. (2013). Direct transfer of graphene onto flexible substrates. *Proceedings of the National Academy of Sciences*, 110(44), 17762–17767. <http://dx.doi.org/10.1073/pnas.1306508110>. Available from: <http://www.pnas.org/content/110/44/17762.abstract>
- Marton, D., Boyd, K. J., Al-Bayati, A. H., Todorov, S. S., Rabalais, J. W. (1994). Carbon Nitride Deposited Using Energetic Species: A Two-Phase System. *Physical Review Letters*, 73(1), 118–121. Available from: <http://link.aps.org/doi/10.1103/PhysRevLett.73.118>
- Matloob, M. H., Roberts, M. W. (1977). Electron spectroscopic study of nitrogen species adsorbed on copper. *Journal of the Chemical Society, Faraday Transactions 1*, 73, 1393. <http://dx.doi.org/10.1039/f19777301393>. Available from: <http://xlink.rsc.org/?DOI=f19777301393>
- Mattevi, C., Kim, H., Chhowalla, M. (2011). A review of chemical vapour deposition of graphene on copper. *Journal of Materials Chemistry*, 21(10),

3324. <http://dx.doi.org/10.1039/c0jm02126a>. Available from:<http://xlink.rsc.org/?DOI=c0jm02126a>

- Mekhalif, Z., Sinapi, F., Laffineur, F., Delhalle, J. (2001). XPS and electrochemical characterisation of polycrystalline copper modified with 12-(N-pyrrolyl)-n-dodecanethiol. *Journal of Electron Spectroscopy and Related Phenomena*, 121(1-3), 149–161. [http://dx.doi.org/10.1016/S0368-2048\(01\)00332-2](http://dx.doi.org/10.1016/S0368-2048(01)00332-2)
- Meyer, J. C., Kurasch, S., Park, H. J., Skakalova, V., Künzel, D., Gross, A., Chuvilin, A., Algara-Siller, G., Roth, S., Iwasaki, T., Starke, U., Smet, J. H., Kaiser, U. (2011). Experimental analysis of charge redistribution due to chemical bonding by high-resolution transmission electron microscopy. *Nature materials*, 10(3), 209–215. <http://dx.doi.org/10.1038/nmat2941>. Available from:<http://www.ncbi.nlm.nih.gov/pubmed/21240288><http://dx.doi.org/10.1038/nmat2941>
- Miniussi, E., Pozzo, M., Baraldi, a., Vesselli, E., Zhan, R. R., Comelli, G., Menteş, T. O., Niño, M. a., Locatelli, a., Lizzit, S., Alfè, D. (2011). Thermal stability of corrugated epitaxial graphene grown on Re(0001). *Physical Review Letters*, 106(21), 2–5. <http://dx.doi.org/10.1103/PhysRevLett.106.216101>
- Miyata, Y., Kamon, K., Ohashi, K., Kitaura, R., Yoshimura, M., Shinohara, H. (2010). A simple alcohol-chemical vapor deposition synthesis of single-layer graphenes using flash cooling. *Applied Physics Letters*, 96(26), 263105. <http://dx.doi.org/10.1063/1.3458797>. Available from:<http://link.aip.org/link/APPLAB/v96/i26/p263105/s1&Agg=doi>
- Moulder, J., Stickle, W., Sobol, P., Bomben, K. (1992). Handbook of X-ray photoelectron spectroscopy. *Perkin-Elmer Corp, Eden Prairie*.
- Nandamuri, G., Roumimov, S., Solanki, R. (2010). Chemical vapor deposition of graphene films. 145604. <http://dx.doi.org/10.1088/0957-4484/21/14/145604>
- Novoselov, K. S., Fal'ko, V. I., Colombo, L., Gellert, P. R., Schwab, M. G., Kim, K., Fal'ko, V. I., Colombo, L., Gellert, P. R., Schwab, M. G., Kim, K. (2012). A roadmap for graphene. *Nature*, 490(7419), 192–200. <http://dx.doi.org/10.1038/nature11458>. Available from:<http://www.ncbi.nlm.nih.gov/pubmed/23060189><http://dx.doi.org/10.1038/nature11458>
- of Iowa, U. Scanning Electron Microscopy. Available from:<http://cmrf.research.uiowa.edu/scanning-electron-microscopy>
- Palsson, M. (2003). *Raman Spectroscopy and Confocal Raman Imaging*. Lund University Libraries.

- Panchokarla, L. S., Subrahmanyam, K. S., Saha, S. K., Govindaraj, A., Krishnamurthy, H. R., Waghmare, U. V. Rao, C. N. R. (2009). Synthesis, Structure, and Properties of Boron- and Nitrogen-Doped Graphene. *Advanced Materials*, *21*, 4726–4730. <http://dx.doi.org/10.1002/adma.200901285>. Available from:<GotoISI>://WOS:000273204200013
- Pels, J., Kapteijn, F., Moulijn, J., Zhu, Q. Thomas, K. (1995). Evolution of nitrogen functionalities in carbonaceous materials during pyrolysis. *Carbon*, *33*(11), 1641–1653. [http://dx.doi.org/10.1016/0008-6223\(95\)00154-6](http://dx.doi.org/10.1016/0008-6223(95)00154-6). Available from:<http://www.sciencedirect.com/science/article/pii/0008622395001546>
- Pimenta, M. a., Dresselhaus, G., Dresselhaus, M. S., Cançado, L. G., Jorio, a. Saito, R. (2007). Studying disorder in graphite-based systems by Raman spectroscopy. *Physical chemistry chemical physics : PCCP*, *9*(11), 1276–91. <http://dx.doi.org/10.1039/b613962k>. Available from:<http://www.ncbi.nlm.nih.gov/pubmed/17347700>
- Point, S., Minea, T., Bouchet-Fabre, B., Granier, A. Turban, G. (2005). XPS and NEXAFS characterisation of plasma deposited vertically aligned N-doped MWCNT. *Diamond and Related Materials*, *14*(3-7), 891–895. <http://dx.doi.org/10.1016/j.diamond.2004.10.011>. Available from:<http://www.sciencedirect.com/science/article/pii/S0925963504003693>
- Qu, L., Liu, Y., Baek, J. B. Dai, L. (2010). Nitrogen-doped graphene as efficient metal-free electrocatalyst for oxygen reduction in fuel cells. *ACS Nano*, *4*, 1321–1326. <http://dx.doi.org/10.1021/nn901850u>
- Reich, S. Thomsen, C. (2004). Raman spectroscopy of graphite. *Philosophical transactions. Series A, Mathematical, physical, and engineering sciences*, *362*(1824), 2271–88. <http://dx.doi.org/10.1098/rsta.2004.1454>. Available from:<http://www.ncbi.nlm.nih.gov/pubmed/23505324>
- Reina, A., Jia, X., Ho, J., Nezich, D., Son, H., Bulovic, V., Dresselhaus, M. S. Kong, J. (2009). Large area, few-layer graphene films on arbitrary substrates by chemical vapor deposition. *Nano letters*, *9*(1), 30–5. <http://dx.doi.org/10.1021/nl801827v>. Available from:<http://www.ncbi.nlm.nih.gov/pubmed/19046078>
- Riedl, C., Coletti, C. Starke, U. (2010). Structural and electronic properties of epitaxial graphene on SiC(0001): a review of growth, characterization, transfer doping and hydrogen intercalation. *Journal of Physics D: Applied Physics*, *43*(37), 374009. <http://dx.doi.org/10.1088/0022-3727/43/37/374009>.

Available from:[http://iopscience.iop.org/0022-3727/43/37/374009\\$backslash\\$http://www2.fkf.mpg.de/ga/publications/preprints/Riedl_JPhysD_Graphene_Review_Preprint.pdf](http://iopscience.iop.org/0022-3727/43/37/374009$backslash$http://www2.fkf.mpg.de/ga/publications/preprints/Riedl_JPhysD_Graphene_Review_Preprint.pdf)

- Rivoal, J.-C. Frétiigny, C. (2005). Microscopie à force atomique (AFM). *Techniques de l'ingénieur Mesures tridimensionnelles et états de surface*, (ref. article : r1394). Available from:<http://www.techniques-ingenieur.fr/base-documentaire/mesures-analyses-th1/mesures-tridimensionnelles-et-etats-de-surface-42409210/microscopie-a-force-atomique-afm-r1394/>
- Ronning, C., Feldermann, H., Merk, R., Hofsäss, H., Reinke, P.Thiele, J.-U. (1998). Carbon nitride deposited using energetic species: A review on XPS studies. *Physical Review B*, 58(4), 2207–2215. Available from:<http://link.aps.org/doi/10.1103/PhysRevB.58.2207>
- Shin, H.-J. J., Kim, S. M. S. J., Yoon, S.-M. M., Benayad, A., Kim, K. K., Kim, S. M. S. J., Park, H. K., Choi, J.-Y. Y., Lee, Y. H., Soo, M. K., Yoon, S.-M. M., Benayad, A., Ki, K. K., Sung, J. K., Hyun, K. P., Choi, J.-Y. Y. Young, H. L. (2008). Tailoring Electronic Structures of Carbon Nanotubes by Solvent with Electron-Donating and -Withdrawing Groups. *Journal of the American Chemical Society*, 130(6), 2062–2066. <http://dx.doi.org/10.1021/ja710036e>. Available from:<http://dx.doi.org/10.1021/ja710036e>
- Smith, E. Dent, G. (2005). *Modern Raman Spectroscopy: A Practical Approach*. John Wiley & Sons, Ltd.
- Srivastava, A., Galande, C., Ci, L., Song, L., Rai, C., Jariwala, D., Kelly, K. F.Ajayan, P. M. (2010). Novel Liquid Precursor-Based Facile Synthesis of Large-Area Continuous, Single, and Few-Layer Graphene Films. *Chemistry of Materials*, 22(11), 3457–3461. <http://dx.doi.org/10.1021/cm101027c>. Available from:<http://pubs.acs.org/doi/abs/10.1021/cm101027c>
- Srivastava, M., Kumar, M., Singh, R., Agrawal, U. C.Garg, M. O. (2009). Energy-related applications of carbon materials - a review. *Journal of Scientific & Industrial Research*, 68(2), 93–96.
- Sun, Z., Yan, Z., Yao, J., Beitler, E., Zhu, Y.Tour, J. M. (2010). Growth of graphene from solid carbon sources. *Nature*, 468(7323), 549–552. <http://dx.doi.org/10.1038/nature09804>. Available from:<http://www.ncbi.nlm.nih.gov/pubmed/21068724><http://dx.doi.org/10.1038/nature09579><http://dx.doi.org/10.1038/nature09804>
- Sutter, P., Sadowski, J. T.Sutter, E. (2009). Graphene on Pt(111): Growth and substrate interaction. *Physical Review B*, 80(24), 245411. Available from:<http://>

[//link.aps.org/doi/10.1103/PhysRevB.80.245411](http://link.aps.org/doi/10.1103/PhysRevB.80.245411)

- Usachov, D., Vilkov, O., Grüneis, A., Haberer, D., Fedorov, A., Adamchuk, V. K., Preobrajenski, A. B., Dudin, P., Barinov, A., Oehzelt, M., Laubschat, C., Vyalikh, D. V. (2011). Nitrogen-doped graphene: efficient growth, structure, and electronic properties. *Nano Letters*, *11*(12), 5401–5407. <http://dx.doi.org/10.1021/nl2031037>. Available from: <http://www.ncbi.nlm.nih.gov/pubmed/22077830>
- Wang, H., Maiyalagan, T., Wang, X. (2012). Review on Recent Progress in Nitrogen-Doped Graphene: Synthesis, Characterization, and Its Potential Applications. *ACS Catalysis*, *2*(5), 781–794. <http://dx.doi.org/10.1021/cs200652y>. Available from: <http://dx.doi.org/10.1021/cs200652y>
- Watts, J. F., Wolstenholme, J. (2003). *An Introduction to Surface Analysis by XPS and AES 1st Edition*. Wiley. <http://dx.doi.org/10.1002/0470867930>
- Wei, D., Liu, Y., Wang, Y., Zhang, H., Huang, L., Yu, G. (2009). Synthesis of n-doped graphene by chemical vapor deposition and its electrical properties. *Nano Letters*, *9*(5), 1752–1758. <http://dx.doi.org/10.1021/nl803279t>
- Wu, T., Shen, H., Sun, L., Cheng, B., Liu, B., Shen, J. (2012). Nitrogen and boron doped monolayer graphene by chemical vapor deposition using polystyrene, urea and boric acid. *New Journal of Chemistry*, *36*(6), 1385. <http://dx.doi.org/10.1039/c2nj40068e>. Available from: <http://xlink.rsc.org/?DOI=c2nj40068e>
- Yan, K., Peng, H., Zhou, Y., Li, H., Liu, Z. (2011). Formation of Bilayer Bernal Graphene: Layer-by-Layer Epitaxy via Chemical Vapor Deposition. *Nano Letters*, *11*(3), 1106–1110. <http://dx.doi.org/10.1021/nl104000b>. Available from: <http://dx.doi.org/10.1021/nl104000b>
- Zhang, C., Fu, L., Liu, N., Liu, M., Wang, Y., Liu, Z. (2011). Synthesis of nitrogen-doped graphene using embedded carbon and nitrogen sources. *Advanced materials (Deerfield Beach, Fla.)*, *23*(8), 1020–4. <http://dx.doi.org/10.1002/adma.201004110>. Available from: <http://www.ncbi.nlm.nih.gov/pubmed/21341318>
- Zhang, W. J., Zhang, Q. F., Chai, Y., Shen, X., Wu, J. L. (2007). Carbon Nanotube Intramolecular Junctions. *Nanotechnology*, *18*(39), 395205. <http://dx.doi.org/10.1088/0957-4484/18/39/395205>